AD-A081 612   NAVAL POSTGRADUATE SCHOOL MONTEREY CA   F/G 21/5
              ATMOSPHERIC DISPERSION OF HIGH VELOCITY JETS.(U)
              NOV 79 J V BRENDMOEN, D W NETZER
UNCLASSIFIED NPS-67-79-012   NL
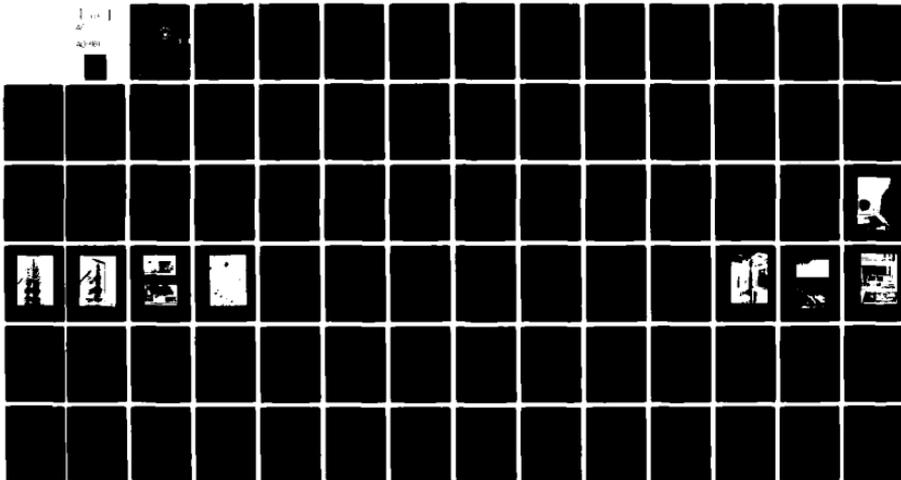
END
DATE
FILMED
4 80
DTIC

LEVEL *II* 2

ADA081612

NAVAL POSTGRADUATE SCHOOL
Monterey, California

DTIC
S ELECTE
MAR 1 1 1980

_A_

Final rpt.

NAVAL POSTGRADUATE SCHOOL REPORT

Atmospheric Dispersion of High Velocity Jets.

by

Jack V. Brendmoen

David W. Netzer

Nov 79 | 83

F57572

ZF57572401

80 3 10 134

251450

DDC FILE COPY

NAVAL POSTGRADUATE SCHOOL

Monterey, California

Rear Admiral T. F. Dedman   Jack R. Borsting
Superintendent   Provost

This report was prepared by:
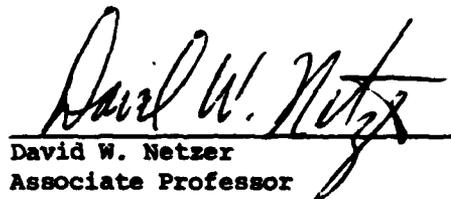
Jack V. Brendmoen   David W. Netzer
LT., USN   Associate Professor

Reviewed by: Released by:

M. F. PLATZER, Chairman   W. M. TOLLES
Department of Aeronautics   Dean of Research

REPORT DOCUMENTATION PAGE		READ INSTRUCTIONS BEFORE COMPLETING FORM
1. REPORT NUMBER NPS 67-79-012	2. GOVT ACCESSION NO.	3. RECIPIENT'S CATALOG NUMBER
4. TITLE (and Subtitle) Atmospheric Dispersion of High Velocity Jets		5 TYPE OF REPORT & PERIOD COVERED Final
		6. PERFORMING ORG. REPORT NUMBER
7. AUTHOR(s) Jack V. Brendmoen David W. Netzer		8. CONTRACT OR GRANT NUMBER(s)
9. PERFORMING ORGANIZATION NAME AND ADDRESS Naval Postgraduate School Monterey, California 93940		10. PROGRAM ELEMENT, PROJECT, TASK AREA & WORK UNIT NUMBERS 62765N; ZF57-572-002 N6237679WR00014
11. CONTROLLING OFFICE NAME AND ADDRESS Naval Air Propulsion Center Trenton, New Jersey 08628		12. REPORT DATE November 1979
		13. NUMBER OF PAGES 72
14. MONITORING AGENCY NAME & ADDRESS(if different from Controlling Office)		15. SECURITY CLASS. (of this report)
		15a. DECLASSIFICATION/DOWNGRADING SCHEDULE

16. DISTRIBUTION STATEMENT (of this Report)

Approved for public release; distribution unlimited

17. DISTRIBUTION STATEMENT (of the abstract entered in Block 20, if different from Report)

18. SUPPLEMENTARY NOTES

19. KEY WORDS (Continue on reverse side if necessary and identify by block number)

Air Pollution
Jet Dispersion

20. ABSTRACT (Continue on reverse side if necessary and identify by block number) A neutrally stable atmospheric surface layer was simulated in a low speed wind tunnel by tripping the boundary layer with a fence and letting the turbulent flow develop over a length of roughness elements. Turbojet exhaust dispersion characteristics, simulated by a burner/nozzle system, were investigated by measuring the horizontal and vertical temperature profiles at axial stations downwind from the nozzle exit. Dispersion sensitivity to different nozzle exit conditions, angles of incidence to the wind, and nozzle surface blockage were investigated. The results were compared to dispersion methods used in the Air Quality Assessment Model (AQAM). It was

DD FORM 1473 EDITION OF 1 NOV 65 IS OBSOLETE
S/N 0102-014-6601

i

found that (1) the experimental jet penetration length was much shorter than that assumed in AQAM, (2) the horizontal jet exhibited plume rise, (3) the initial dispersion coefficients were a function of wind direction, and (4) the plume spreading rate was more rapid than for low velocity, elevated sources in neutrally stable atmospheric conditions.

TABLE OF CONTENTS

LIST OF TABLES

LIST OF FIGURES

TABLE OF SYMBOLS

JD	Jet Diameter
p	Pressure
$T\sigma$	Temperature at One Standard Deviation from the Mean
u	Average Velocity Component in the x Direction
u'	Fluctuating Velocity Component in the x Direction
u_*	Wall Friction Velocity
U_∞	Free Stream Velocity in the Wind Tunnel
w	Average Velocity Component in the z Direction/Jet Plume Lateral Dimension
w'	Fluctuating Velocity Component in the z Direction
x	Axial Direction
y	Lateral Direction
z	Vertical Direction
z_o	Roughness Length
Δz	Jet Plume Vertical Dimension
κ	Von Karman's Constant
ν	Kinematic Viscosity
ρ	Density
$\overline{\rho u' w'}$	Turbulent Shear Stress
σ	Standard Deviation
σ_{yo}	Initial Dispersion Coefficient in the Lateral Direction
σ_{zo}	Initial Dispersion Coefficient in the Vertical Direction
σ_y	Dispersion Coefficient for the Lateral Direction
σ_z	Dispersion Coefficient for the Vertical Direction
τ_o	Wall Shear Stress
τ	Shear Stress

I. INTRODUCTION

The Air Force has developed an Air Quality Assessment Model (AQAM) to predict the dispersion of pollutants emitted from typical Air Base related sources (Ref. 1, 2 and 3). That model has also been modified to better simulate operations from a Naval Air Station (Ref. 4 and 5). The full model consists of three computer programs: Source Inventory, Short Term and Long Term Dispersion. In the Short Term Model hourly averaged concentrations are predicted over a grid of receptors. Air-base, air-craft, and off air-base (environ) sources are considered and are modeled as point, area, or line sources as appropriate.

In the Short Term Model, the jet exhausts from aircraft during taxi and takeoff are treated as line sources with no plume rise. Initial plume dimensions must be estimated as well as the distance the jet "penetrates" the atmosphere before coming essentially to rest relative to the ambient wind. Stationary sources such as engine run up test stands and test cells are treated as points sources. Likewise, the initial plume dimensions must be estimated and a determination whether plume rise is a factor must be made. The model then uses these input data to determine an initial dispersion coefficient from which a pseudo upwind point or line source is located. The sigma's, or dispersion coefficients, are based on the stability class of the atmosphere and the downwind distance or travel time for an elevated, relatively low velocity source. There is a question then, as to the applicability of these dispersion coefficients to turbojet exhausts which are often sonic, have high shear stress/turbulent mixing characteristics and have different turbulence scales than typical exhaust stacks. Evidence that there is a discrepancy has been

1

indicated by an Air Force study (Ref. 6) which presented a pictorial investigation of the effects of atmospheric stability on a jet exhaust. It is evident that qualitative and quantitative data are needed to characterize the dispersion of a turbojet exhaust during ground operations. This investigation attempted to determine turbojet exhaust dispersion as a function of jet characteristics and wind direction under laboratory simulated, neutrally stable atmospheric conditions.

The first part of the study involved the correct simulation of the lower portion of the atmoshpere in an aeronautical type wind tunnel. Published studies (Refs. 7, 8 and 9) have indicated that it is not sufficient to simulate only the mean velocity profile of the atmosphere. The turbulent structure of the atmosphere must also be correctly modeled simultaneously with the mean velocity profile. Proper simulation can be accomplished following the work of Sundaram and Ludwig (Ref. 7), tripping the boundary layer with a suitable fence at the entrance of the wind tunnel test section and then letting the turbulent flow develop over a length of roughness elements. Suitable matching between the boundary layer trip and the roughness elements then results in an area of constant shear stress which adequately models the atmospheric flow.

Once an atmoshperic surface layer has been suitably simulated, a turbojet exhaust must then be simulated. If it is assumed that heat and mass have the same turbulent diffusion characteristics, then the dispersion rates of pollutants can be determined by measuring the temperature distributions in the vertical and horizontal directions.

In this investigation data were obtained for varying angles of incidence to the oncoming wind for choked and unchoked nozzle flow conditions,

2

for two jet temperatures, and for two conditions of nozzle surface block-

age.   The data were compared to the dispersion routines used in the AQAM

computer program.

II. ATMOSPHERIC SIMULATION

In order to make meaningful wind tunnel measurements to determine
jet aircraft exhaust dispersion rates during taxi, idle and takeoff
modes of operation it was necessary to correctly model the lower struc-
ture of the atmoshpere. Sundaram and Ludwig (Ref. 7) have published a
theoretical study of the requirements for the modeled flow and an ex-
perimental study of the flow generated by wind tunnel techniques. This
reference was used as the principal guide in modeling the atmoshperic
surface layer in a wind tunnel at the Naval Postgraduate School. Sup-
plementary discussions are presented in Refs. 10-12.

A. THEORETICAL REQUIREMENTS FOR ATMOSHPERIC MODELING

Reference 13 describes the atmoshperic boundary layer as a turbulent
layer which is influenced by a combination of actions due to surface
friction, thermal stratification, and Coriolis force. The atmospheric
boundary layer is divided into two distinct layers. The lower region
called the surface boundary layer extends up to a nominal height of 100
meters. The region above the surface layer is called the Ekman layer
and extends up to a height of about 1000 meters. In the surface layer,
the wind direction is generally considered to remain constant and the
Coriolis force is not an important parameter. In an ideal environment
the near-surface region is horizontally homogeneous and free of pressure
gradients. These conditions imply that the shear stress can be considered
to be independent of height in the region close to the surface. Surface
layer theories (Ref. 14) often employ the assumption that the flow char-
acteristics close to the ground can be expressed entirely in terms of

4

conditions at the surface. Most atmoshperic boundary layers are observed
to have no laminar sublayer near the surface and are described to be fully
aerodynamically rough. A turbulent, neutrally stable flow structure in
the atmospheric surface boundary layer can be described entirely by the
following parameters; the kinematic viscosity ν , the friction velocity
u_* , and the roughness parameter z_o (Ref. 7). u_* is defined as being
equal to $(\tau_o/\rho)^{\frac{1}{2}}$ and z_o is a length-scale which describes the influ-
ence of a rough surface on a particular flow.

Using the above parameters, an aerodynamically rough flow exists if
(Ref. 7)

$$z_o u_*/\nu > 3. \tag{1}$$

If z_o is $<<$ than the vertical dimension of the boundary layer, then the
mean-velocity profile of the wind is given in logarithmic form by the re-
lationship (Ref. 7)

$$u/u_* = (1/\kappa) \ln (z/z_o), \tag{2}$$

where u is the average velocity, z is the vertical distance from the
surface and κ is Von Karman's constant. This equation is a form of the
well known law of the wall and is indicative of the interaction between
the air flow above a given surface and that surface.

To accurately model the atmosphere the requirements of aerodynami-
cally rough flow, horizontal homogeneity and the absence of pressure
gradients must be adhered to. Strict horizontal homogeneity, however, is
extremely difficult to obtain in the laboratory. Partial simulation,
therefore, generally has to be imposed. A complete discription of the

5

effects of partial simulation is given in reference 7 and will not be repeated here. The conclusion reached from reference 7 regarding partial simulation was that a laboratory flow which was fully aerodynamically rough, nearly horizontally homogeneous and relatively free from pressure gradients was a reasonable model for a neutrally stable atmosphere. The generation of such a flow is described in the next section of this report.

B. EXPERIMENTAL REQUIREMENTS TO SIMULATE ATMOSPHERIC FLOWS

Aircraft jet exhaust dispersion in the "near ground" environment was the primary concern of this investigation; therefore only the surface layer of the atmosphere was required to be simulated. As discussed previously, this was possible since both the atmospheric flow and the simulated flow are described completely in terms of conditions at the surface (ie. the parameters u_*, z_0, and ν). The similarity requirements were, therefore, not a function of the geostrophic wind in the real flow nor a function of the free stream velocity in the simulated flow. Horizontal homogeneity cannot be strictly satisfied since for an experimental flow over a flat plate, equilibrium conditions change continually as a function of downstream distance (Ref. 7).

Since the atmosphere is assumed to exhibit a logarithmic mean velocity profile and to be horizontally homogeneous, this part of the similarity requirement can be verified by measuring the mean velocity profile at several locations in the wind tunnel flow. In reference 7 the turbulence intensity and the integral scale of turbulence were also measured and compared to available atmospheric data. Turbulence intensity measurements were also made in this experiment and compared to the results of reference

6

7. Integral scales of turbulence were not measured. For virtually identical experimental set-ups it was assumed that if all other experimental measurements compared favorable to those of reference 7, then the scales of turbulence would also compare favorably.

C. EXPERIMENTAL APPARATUS AND MEASUREMENTS

1. Wind Tunnel Modifications

The experiment was conducted in a low speed wind tunnel at the Naval Postgraduate School (NPS), Monterey, CA. The wind tunnel draws ambient air from the surrounding area into a 5 X 5 foot test section approximately 21 feet long. In order to be comparable with the wind tunnel used in reference 7, the wind tunnel at the Naval Postgraduate School was modified in the following manner. A false ceiling was installed to maintain an approximate zero pressure gradient in the axial direction. A two inch high boundary layer trip constructed of wood was placed across the entrance to the test section. The trip was followed by 2.5 X 2.5 feet square sections of roughness elements which covered the entire floor of the test section. The roughness elements were 4 sided regular pyramids which were 0.75 inches square at the base and 0.75 inches in height. They were constructed out of 1.5 inch thick fiberboard. The tunnel and roughness elements are shown in figure 1.

2. Pressure Measurements

Six, 1/8 inch diameter pressure taps spaced 4 feet apart, were mounted flush along the centerline of the wind tunnel wall. The differential area required to maintain a zero pressure gradient in the axial direction was determined from an initial set of pressure readings. The false

7

ceiling which implemented the required area change was then installed and the pressure readings were again taken to verify the required zero axial pressure variation.

3. Electronic Equipment

All velocity related measurements were taken with a Thermo Systems Inc. linearized hotwire anemometer system. DISA single wire and cross wire probes and probe holders were used with the anemometer system (fig. 2 and 3). A DC digital voltmeter and a true RMS meter were used to record the steady and fluctuating single wire probe data respectfully. A model 1015C Thermo Systems Inc. correlator was used in conjunction with the cross wire outputs to obtain the sum and difference of the two signals (fig. 4). The true RMS meter was also used to record the cross wire outputs via the correlator. The hotwire probes were mounted under the wind tunnel such that the probes traversed the wind tunnel in a vertical direction. A Spectral Dynamics, Spectra-Scope Model SD-330 frequency counter was used in conjunction with the measurement of the centerline velocity (fig. 5).

4. Wind Tunnel Centerline Velocity Measurements

The maximum velocity expected in the wind tunnel was between 40 and 50 feet per second. Existing pitot-static systems at NPS were not sensitive to this small velocity. Therefore, the relationship between the Strouhal Number and the Reynolds Number was used to determine the center-line velocity (Ref. 15). The Strouhal number relates the velocity of a flow to the frequency at which vortices are shed behind a circular cylinder which is immersed in that flow.

Sn(Strouhal Number) = (freq. X diam. of cyl.) / velocity.

8

A 0.075 inch diameter stainless steel wire was attached to a collar which was fitted over a single hotwire probe such that the hotwire was in only one wake (shed vortex sheet) of the cylinder (fig. 6). The probe, collar and hotwire combination was placed perpendicular to the flow at the center-line of the tunnel. With the tunnel on, the hotwire system was sensitive to the velocity of the free stream and the output was observed and recorded on the frequency counter. The observed frequency of shed vorticies and the unique relationship between the Strouhal Number and the Reynolds Num-ber were used to iteratively determine the velocity of the free stream.

5. Velocity Profile Measurements

The mean velocity profile measurements were made using the single hotwire apparatus. The hotwire system was calibrated in the linear mode such that the centerline velocity was made equal to one volt. The single wire was also calibrated for flow direction sensitivity. This was accomplished by rotating the probe until a maximum reading was observed on the DC digital voltmeter. It was then assumed that the probe was perpen-dicular to the flow. All subsequent measurements were referenced to this direction. The linearized output was averaged through a ten second time constant before being displayed on the DC digital voltmeter. The velocity profile was obtained by recording the DC value of the hotwire output as it traversed the wind tunnel in the vertical direction. Vertical measurements were referenced to the top of the roughness elements and were measured to within an accuracy of 0.020 inches with respect to that reference. Veloci-ty profiles were obtained at two axial locations. The locations were 72 inches and 109 inches downwind from the boundary layer trip at the entrance to the test section. The two axial measurements were necessary to ensure the required degree of uniformity in the jet dispersion region.

6. Turbulence/Shear Stress Measurements

The cross wire system described earlier was used to measure the turbulence intensities and shear stresses directly. The cross wire was calibrated such that the linearized output for each wire was of equal sensitivity. This was accomplished by first orienting one wire normal to the flow and then adjusting its sensitivity to the proper level. The probe was then re-oriented so that the second wire was normal to the flow and its sensitivity was then matched to that of the first wire. For data acquisition, the probe was oriented axially such that the longitudinal turbulence intensity was proportional to the RMS value of the sum of the cross wire outputs. Likewise, for the same orientation, the vertical turbulence intensity was proportional to the RMS value of the difference of the cross wire outputs. The turbulent shear stress is defined as $-\rho\overline{u'w'}$. This shear stress was obtained directly since $\overline{u'w'}$ is proportional to the square of the sum minus the square of the difference of the cross wire outputs. Like the single wire data, the cross wire data was recorded as the probe was traversed in the vertical direction at the same two axial locations. For redundancy, the vertical profile of turbulence intesnity was also measured using the single wire probe.

D. RESULTS AND DISCUSSION

All the measurements obtained at the two axial locations, ie. 72 and 109 inches from the entrance of the wind tunnel test section, were taken with a wind tunnel center line velocity of approximately 40 feet per second.

1. $\underline{u_* \text{ and } z_o}$

From the law of the wall,

$$u/u_* = 5.75 \log z/z_o \tag{3}$$

Equation (3) can be rewritten as

$$u/U_\infty = (u_*/U_\infty) \, 5.75 \, (\log z - \log z_o). \tag{4}$$

When u/U_∞ is plotted vs. $\log z$,

$$\text{slope} = 5.75 \, (u_*/U_\infty). \tag{5}$$

u/U_∞ vs. $\log z$ was plotted for both axial positions and a least squares fit was obtained through the data points (figures 7 and 8). The slopes were measured and u_* was determined by;

$$u_* = (\text{slope} \bullet U_\infty)/5.75. \tag{6}$$

u_* values of 2.32 and 2.52 feet per second were obtained at the 72 and 109 inch positions respectively. Using the least squares fit data, the calculated u_* was used to determine z_o by;

$$\log z_o = \log z - u/(5.75 \bullet u_*) \tag{7}$$

z_o values of 0.0215 and 0.0326 were obtained at 72 and 109 inches respectively.

2. Vertical Distribution of Shear Stress

Since u_* is proportional to the shear stress,

$$u_* = \sqrt{\tau_o/\rho} = \sqrt{-\rho \overline{u'w'}/\rho} = \sqrt{\overline{u'w'}} \, , \tag{8}$$

a measure of the average shear stress for each position can be obtained from the mean velocity profile data. Non-dimensionalizing by U_∞^2 ;

$$\overline{u'w'} / U_\infty^2 = (u_*/U_\infty)^2 \tag{9}$$

11

The measured shear stress, $\overline{u'w'}$, from the cross wire data, was also non-dimensionalized by U_∞^2 and plotted as a function of the vertical distance above the roughness elements for both axial positions. Figure 9 presents the cross-wire data. Also shown are the values of average stress determined from the law of the wall.

Figures 10 and 11 compare the results with those presented in reference 7. It is observed that the shear stress continued to increase until very near the wall whereas the shear stress from reference 7 began to decay further from the wall. Figure 10 shows that the shear stress was approximately constant for heights from 2 to 5 inches above the roughness elements at the 72 inch position. At the 109 inch position (fig. 11), the shear stress decayed gradually from the near wall region. In an attempt to modify the near wall shear stress distribution, different combinations of trip heights and wind speeds were tried. This proved to be unsuccessful. The mean velocity profile was observed to vary much more rapidly in the axial direction and the relatively constant shear stress region obtained with the two inch trip was destroyed in varying degrees depending on which trip or what tunnel speed was used. There was also a somewhat greater variation in horizontal homogeneity in this experiment relative to reference 7. This was reflected in the increased slope of figure 8 over that of figure 7. This was also reflected in figure 9 by noting that the average shear stress differed by about 20 percent between the two positions. Moreover, z_o increased by about 50 percent over the axial range compared to about 30 percent for the experiment of reference 7. It was also noted in reference 7, however, that the degree of uncertainty in the atmosphere may be much larger than the 30 percent figure.

12

3. Vertical and Horizontal Turbulence Intensities

Figures 12 and 13 compare the measured vertical and horizontal turbulence intensity measurements at the two axial locations with the of reference 7. In general, the vertical and horizontal data agree extremely well with the data of reference 7. The horizontal turbulence a little lower for both positions in the range of z/z_o from 40. This corresponded to a a height of about one inch above the elements and was the area of difference noted in figures 10 and 11.

Since, (1) a region of constant shear stress was obtained in agreement with reference 7, (2) the turbulence intensities were rel constant over the same region, (3) the roughness parameter z_o was parable to that of reference 7, and (4) equation (1) was satisfied, the simulated atmoshperic surface layer was considered to be adequate initial study of jet exhaust dispersion.

III. SIMULATED JET DISPERSION IN A WIND TUNNEL

A. BACKGROUND

The AQAM model treats most aircraft emissions as finite line sources. Aircraft engine test cells and run up stands are treated as point sources. Line sources are modeled by a general line source or puff type model (Ref. 1-3). Point sources are modeled by the application of Gaussian plume theory. This theory represents the downwind concentration of pollutants from an elevated source as Gaussian distributions in both the horizontal and vertical directions. When applied to aircraft exhausts, the line source method first assumes that the emissions from the moving aircraft come to rest relative to the ambient wind after a penetration length due to the velocity effects of the jet. After coming to rest, the source of finite cross-section is generally segmented. The segmented portions of the source are then assumed to behave as pseudo-upwind line sources which are dispersed downwind in a Gaussian manner. Point and line sources both employ the same dispersion coefficients σ_y and which are the standard deviation points of a Gaussian or normal distribution curve and are described by Turner in his workbook on dispersion estimations (Ref. 16). As mentioned earlier, the dispersion coefficients are based on the atmospheric stability class and the time or distance traveled downwind from a relatively low velocity source. The application of these coefficients relative to a high velocity, horizontally emitted source, such as a turbojet engine, was investigated for various jet parameters.

14

B. EQUIPMENT

1. General Discussion

The investigation was conducted in the low speed wind tunnel described in the previous section. A burner/nozzle assembly provided the simulated turbojet exhaust. The temperatures within the exhaust were measured in the vertical and horizontal directions using a thermocouple apparatus.

2. Burner/Nozzle

Oxygen and ethylene were mixed and ignited at the entrance to a burner can, figure 14. The hot gases were diluted with air to provide burner cooling and the desired flow rates. The burner exhausted into the wind tunnel through a 1/8 inch diameter stainless steel tube. The tube was inserted through the tunnel floor. It was made with one 90 degree bend which aligned the exhaust parallel to the tunnel floor. A nozzle was created by reducing the exit diameter of the tubing to 0.058 inches. The tube was positioned 3 inches above the roughness elements. This position was chosen since it was about the center of the area of constant shear stress discussed in the atmospheric simulation section of this report. Stagnation pressure and temperature probes were used to determine the nozzle exit conditions. The nozzle entered the wind tunnel at a position 72 inches downstream from the boundary layer trip described in the previous section.

3. Temperature Measuring

Horizontal and vertical temperature profiles were obtained using a chromel-alumel thermocouple probe. The thermocouple was referenced to an Omega electronic Miniature Cold Junction (MCJ). The nozzle and

thermocouple system is shown in figure 15. A probe holder and a traverse system permitted positioning of the thermocouple probe in varying axial, transverse, and vertical locations. The traverse system, an electrical-mechanical device mounted under the wind tunnel (fig. 16), facilitated positioning in the vertical and transverse direction. The probe holder, mounted on the traverse system, permitted the thermocouple probe to be positioned in the axial direction. Two X-Y plotters (fig. 17) were used to record the temperature profiles as a function of downwind distance. One plotter was used for the vertical temperature profile and the other for the horizontal temperature profile.

C. DISCUSSION OF RESULTS

1. Introduction

The dispersion data from the experimental jet exhaust were used to determine 1) if the plume dispersion was Gaussian, 2) the sensitivity of the jet dispersion to the wind direction, 3) the sensitivity of the jet exhaust dispersion to nozzle exit Mach number (choked and unchoked) under no-wind and wind conditions, 4) the sensitivity of the jet dispersion to upwind nozzle surface blockage and 5) the effect of increased jet exhaust exit temperature on plume rise. The first four items were investigated with an exhaust stagnation temperature of 550 degrees F while the stagnation temperature for the plume rise investigation was increased to 700 degrees F. For choked flow the exhaust stagnation pressure was 32 psia. For unchoked flow it was 22 psia.

2. Attainment of Gaussian Dispersion

A Gaussian or normal distribution with a mean value of zero is defined by the equation

16

$$y = \{1/(\sqrt{2\pi}\sigma)\} \quad \exp[-.5(x/\sigma)^2]. \tag{10}$$

A standard normal distribution (fig. 18) is a normal distribution in which σ is set equal to one. In this case, the maximum value of the ordinate of equation 10 is $1/\sqrt{2\pi}$ or 0.3989. The value of the ordinate at one standard deviation, where $x = \sigma$, of equation 10 is 0.242. To determine whether the measured temperature profiles were Gaussian the profiles were standardized in the following manner. For any measured temperature profile the peak temperature (Tmax) was assumed to be at the mean of the distribution. That temperature was scaled such that Tmax/C was equal to 0.3989. The ordinate values of the temperature profile were then scaled by the factor C. The ordinate value of the one σ point, T_σ, of the profile was determined by; $T_\sigma = C \cdot 0.242$. At this temperature the width of the temperature plume is equal to 2σ. The standard deviation which was determined in this manner was used to non-dimensionalize or standardize the abscissa of the temperature profile. The standard deviations are tabulated in Tables I, II and III for each of the conditions of the experiment. The standardized data points were then plotted against a standard normal distribution curve and compared for closeness of fit. Figures 19 through 24 compare the vertical and horizontal temperature profiles for a choked nozzle flow to the standard normal distribution curve. The jet exhaust was oriented at zero degrees incidence to the free stream wind direction. The wind tunnel centerline velocity was 40 feet per second. The different sets of data represent measurements taken at different axial positions downwind from the jet exhaust. The downwind distance was expressed in terms of jet diameters. The plume was near Gaussian after approximately eight jet diameters downstream from the exit plane of the

17

jet for both the horizontal and vertical profiles. The distance required for the profile to become Gaussian appeared to be the result of the expansion process of the fluid as it exited the nozzle. Similar plots were obtained for the other zero incidence conditions shown in Tables I and II. For each case the plume exhibited near Gaussian properties at about eight jet diameters downstream. The dashed line on Tables I and II indicate the position at which the plume exhibited Gaussian characteristics.

As the nozzle was rotated to the wind direction, the jet-wind interactions caused the horizontal profile to be negatively skewed. The degree of skewness diminished as a function of downwind distance as the effect of the jet exit velocity was overcome by the force of the wind. At the point where the wind was the dominant dispersion factor (ie. past the penetration length) the plume again exhibited Gaussian characteristics. Figure 25 compares the data obtained at an axial distance of 1.72 jet diameters for different angles of incidence to the wind. The angles investigated were 29, 45, 67 and 90 degrees and the data were non-dimensionalized in the same manner as discussed previously. The degree of skewness in figure 25 is evident for each angle of incidence when data are compared to the standard normal distribution curve. Similar data for different downwind stations are plotted on figures 26 through 32. The vertical temperature profiles exhibted no skewness and were very nearly Gaussian at each data position. The σ's which were obtained for the vertical and horizontal dispersions are tabulated in Table III. The downwind distance at which the plume became Gaussian is indicated for each angle by a dotted line.

18

3. Sensitivity of Exhaust Dispersion to Angle

   of Incidence to the Wind

   A spatial representation of the jet exhaust as a function of down-
wind and horizontal distances from the centerline of the nozzle is plot-
ted on figure 33 for jet exhaust angles of incidence to the wind of 29,
45, 67 and 90 degrees. As expected, as the angle of incidence was in-
creased, the length normal to the wind direction where the dispersion di-
tribution was essentially uniform (ie. sigma approaches infinity) incre
(in a nonlinear relationship, fig. 34). The downwind distance at whi
the plume became approximately uniformly distributed was extremely sensi-
tive to the angle of incidence. The downwind distance decreased quite
rapidly as the angle of incidence was increased in an almost linear re-
lationship (fig. 34). From Table III it can also be seen that the
corresponding sigmas increased considerably. Quantitative data was
attempted for angles of incidence greater than 90 degrees. The prob
could not be translated further upstream than the 90 degree jet orienta-
tion. At this position, the exhaust of the jet was completely disperse
Qualitatively then, as the angles of incidence were increased, the exit
jet momentum and wind action acted together to rapidly disperse the ex-
haust in the downwind direction. The dispersion coefficients were in-
creased which resulted in a decreased downwind distance where the plume
became uniformly distributed.

4. Sensitivity of Dispersion Rate to Nozzle Exit Mach Number

   (choked and unchoked), for Wind and No-wind Conditions

   Table I presents the results in terms of the size of the one
standard deviation point of the plume in jet diameters as a function of

19

downwind distance from the nozzle exit. It can be seen that the plume dimensions were relatively insensitive to varying exit conditions (choked, unchoked and high temperature). The data for the unchoked nozzle-with-wind dispersed about the same as did the choked flow. For choked flow the Mach number at the exit was 1.0. For the unchoked flow the Mach number was about 0.8. Therefore, both had high velocities relative to a typical stack exhaust.

The dispersions from a choked nozzle with and without wind were also measured. The two sets of data for both the horizontal and vertical directions are plotted in figures 35 and 36. It is seen that the dispersion of the plume became affected by the wind structure at about 30 jet diameters downwind from the nozzle exit. Between the nozzle exit and about 30 jet diameters downstream, the no-wind and wind data compare fairly well with each other. Further downwind from that position, however, the two curves diverge. It was apparent then that the exit conditions of the nozzle (ie. the penetration length) governed the dispersion of the plume for about the first 30 jet diameters downwind, and thereafter the dispersion was primarily a function of the environmental conditions.

5. Effect of Nozzle Surface Blockage

To investigate the effect of flow disturbances (caused by the tubing upwind of the nozzle) on the dispersion of the jet exhaust, two different non-heat conducting disks were separately fitted on the nozzle tubing. These blockage devices increased the upstream area relative to the 1/8 inch tubing by a factor of 15 and 75 respectfully. Table II contains the results and it was observed that upstream blockage did not greatly affect the dispersion rates. These upstream blockage effects

20

were apparently dissipated by the time that the jet had penetrated approximately 30 jet diameters aft of the nozzle. These data indicate that aircraft configuration may not significantly affect the jet dispersion for the slowly moving taxi operation.

6. Sensitivity to Increased Exit Temperature

As stated previously, the effect of exit temperature had little effect on the plume dimensions as a function of downwind distance. An investigation of the plume rise was conducted by measuring the vertical distance between the peak point of the temperature profile and the centerline of the nozzle for two exhaust temperatures. The two sets of data are compared as a function of downwind distance in figure 37. Because of the small distances it was difficult to make accurate quantitative conclusions with respect to the plume rise. From the data, however, it appeared that the plume rise was about one jet diameter per 100 degrees F change in exit temperature. Equally as interesting as the plume rise was what appeared to be a small degree of looping caused by the turbulent structure of the atmosphere. This phenomenon is shown in figure 37 as a dotted line.

D. COMPARISON OF EXPERIMENTAL RESULTS WITH AQAM

The line source dispersion employed for aircraft exhaust jets in AQAM first assumes that the jet exhaust has a penetration length equal to 140 meters (ie. approximately 140 jet diameters). The penetration length is that length where the velocity effects of the exhaust cease to be a factor in dispersing the exhaust. Thus, the exhaust essentially comes to rest with respect to the ambient air mass. At this distance then, the exhaust is being dispersed entirely by the action of the wind.

In AQAM, estimates of the lateral and vertical dimensions of the

aircraft plume are made at the penetration length. The lateral width w, and vertical height Δz then define the dimensions of a line source of length L. The lateral width is assumed to remain constant over the length of the line. Once the line source has been defined, the line is generally segmented and dispersed downwind using the Gaussian theory of dispersion. That is; 'from the dimensions of the line source an initial σ_{yo} and σ_{zo} are determined from empirical relationships $\sigma_{yo} = w/2.4$ and $\sigma_{zo} = \Delta z/2.4$ respectively. With these values of σ_{yo} and σ_{zo} an up-wind distance for a pseudo upwind line source is determined using the σ_{yo} and σ_{zo} vs. distance or time charts. The pollution concentrations are then dispersed from the determined line source in a Gaussian manner. If w and Δz are not specified inputs, the AQAM model uses default values of 20 meters and 8 meters respectfully.

The penetration length determined in this investigation for zero degrees orientation to the wind was approximately 30 jet diameters, considerably shorter than the 140 jet diameters used in AQAM. The 30 jet diameter figure was further investigated using the dispersion data from tests with the nozzle oriented at other than zero degrees to the wind (fig. 38). The 30 jet diameter penetration distance determined from the axial conditions, indicated by an arc in figure 38, was compared to the point where the dispersion curves exhibited no skewness (ie. where the distributions were Gaussian normal to the wind direction). It was assumed that beyond this position the jet effects could be neglected and that the jet would be dispersed by the ambient wind only. This assumption is not entirely correct since the plume continued to exhibit horizontal displacements normal to the wind. Along the jet axis the

penetration length increased as a function of incidence to the wind from about 28 to 58 jet diameters, still considerably less than the 140 jet diameters assumed by AQAM. This relationship is plotted in figure 39 and appears to be approximately linear between 29 and 90 degrees relative to the axial orientation. The distance downwind from the nozzle where the plume became Gaussian, however, remained approximately constant at 25-30 jet diameters. It was also noted that the corresponding σ's at the Gaussian point for each angle became wider with increased angles of incidence due to more turbulent mixing. This relationship is plotted in figure 40. With the limited number of data points available it appears that the relationship follows a smooth curve. σ_y and σ_z and the jet penetration length seem to be predictable between zero and 90 degrees of incidence to the wind for neutral stability and these nozzle exit conditions. These values could be used in AQAM to determine w and Δz instead of estimating them or using the default values. The relationship shown in figure 39 could also be used as input for jet penetration length. However, since the penetration lengths are small, it may be better to neglect this effect entirely.

A comparison of the rates of dispersion for zero degrees incidence to the wind (i.e. the slopes of the σ_y and σ_z vs. distance curves) was made between those for a neutrally stable atmoshpere (class D) in reference 1 and the experimental data. As can be seen from figures 35 and 36 the experimental dispersion rates were greater than the class D rate used by reference 1 for a neutrally stable atmosphere. Reference 1 indicated that this may be expected. The dispersion rates were obtained from data compiled from typical low velocity stack emissions and not from

23

high velocity sources. In general terms, it appears that for the conditions of this experiment, a more realistic representation of the actual dispersion rate could be obtained if the atmospheric stability class was decreased by one.

For a vertical stack, AQAM also estimates the plume rise due to thermal effects by one of two relationships. These relationships were investigated to see if they could be used to predict the plume rise observed in the experiment. Both Holland and Carson-Moses formulas were found to predict insignificant plume rise for the conditions of this experiment.

IV. SUMMARY AND RECOMMENDATIONS

In summary, a neutrally stable atmospheric surface layer was simulated in a low speed wind tunnel. Horizontal and vertical temperature profiles aft of a converging nozzle were measured. The dispersion rates from the simulated jet exhaust were measured for different nozzle conditions and compared to the dispersion rates used in the AQAM Model. Shorter jet penetration lengths and more rapid jet dispersions were observed. Initial plume dimensions were found to vary significantly with jet orientation to the ambient wind direction and some plume rise was observed.

It is recommended that additional studies be made for conditions of other than neutral stability. Measurements made in less stable surface layers would provide a better understanding of the plume rise and looping phenomena.

σ's Vertical (JD) and σ's Horizontal (JD)

Downwind Distance (JD)	σ's Vertical (JD) wind off choked	σ's Vertical (JD) wind on choked	σ's Vertical (JD) wind on unchoked	σ's Vertical (JD) wind on hi-temp	σ's Horizontal (JD) wind off choked	σ's Horizontal (JD) wind on choked	σ's Horizontal (JD) wind on unchoked	σ's Horizontal (JD) wind on hi-temp
1.72	.574	.574	.862	-	.862	.862	1.0	-
8.62	.862	.862	.862	.862	.862	1.25	1.0	1.0
17.3	1.72	1.44	1.72	2.01	1.72	1.72	2.16	2.16
25.8	2.44	2.29	2.44	2.29	2.16	2.58	2.80	2.70
34.5	3.16	2.90	3.16	3.16	3.87	3.02	3.50	3.40
51.7	4.59	4.02	4.31	4.31	5.60	4.74	5.28	5.30
86.2	8.62	6.61	8.04	6.90	9.48	7.32	8.01	7.75
120.6	10.34	9.19	9.77	10.34	10.7	11.2	11.2	11.0

TABLE I

1-Sigma Plume Width of the Vertical and Horizontal
Temperature Profiles at Zero Degrees Incidence
to the Wind as a Function of Downwind
Distance for Different Nozzle Conditions

		Sigma Vert. (JD) (choked) Blockage			Sigma Horz. (JD) (choked) Blockage		
		none	small	large	none	small	large
	1.72	.574	.574	.574	.862	.862	.862
	8.62	1.00	1.00	1.00	.862	.862	1.29
	17.3	1.43	1.43	1.72	1.72	1.72	1.72
	25.8	2.30	2.30	2.30	2.58	2.60	3.01
	34.5	2.90	3.16	3.44	3.01	3.00	3.87
	51.7	4.02	4.59	4.59	4.74	4.90	5.17
	86.2	6.61	7.04	7.75	7.32	7.50	7.75
	120.6	9.19	9.19	9.19	11.20	11.30	10.34

Downwind Distance JD

Table II

1-Sigma Plume Width of the Vertical and Horizontal
Temperature Profiles at Zero Degrees
Incidence to the Wind for Different
Nozzle Blockages

Sigma Vert. (JD)

Downwind Distance (JD)	0°	29°	45°	67°	90°
1.72	.574	.574	-	-	4.31
8.62	.862	.862	1.15	2.29	6.03
17.3	1.44	1.72	2.29	4.31	9.54
25.8	2.29	2.44	3.45	5.75	-
34.5	2.90	3.16	4.59	7.47	-
51.7	4.02	4.89	6.89	11.49	-
86.2	6.61	8.62	10.91	-	-
120.6	9.19	12.64	-	-	-

Sigma Horz. (JD)

Downwind Distance (JD)	0°	29°	45°	67°	90°
1.72	.862	.287	.574	2.01	11.49
8.62	1.25	.862	1.44	2.87	11.49
17.3	1.72	1.72	3.16	6.32	14.36
25.8	2.58	2.29	4.31	8.33	14.36
34.5	3.02	3.45	5.17	10.15	-
51.7	4.74	5.17	8.04	12.06	-
86.2	7.32	8.04	12.64	-	-
120.6	11.20	11.49	-	-	-

Table III

1-Sigma Plume Width of the Vertical and Horizontal
Temperature Profiles for Different Angles of
Incidence to the Wind
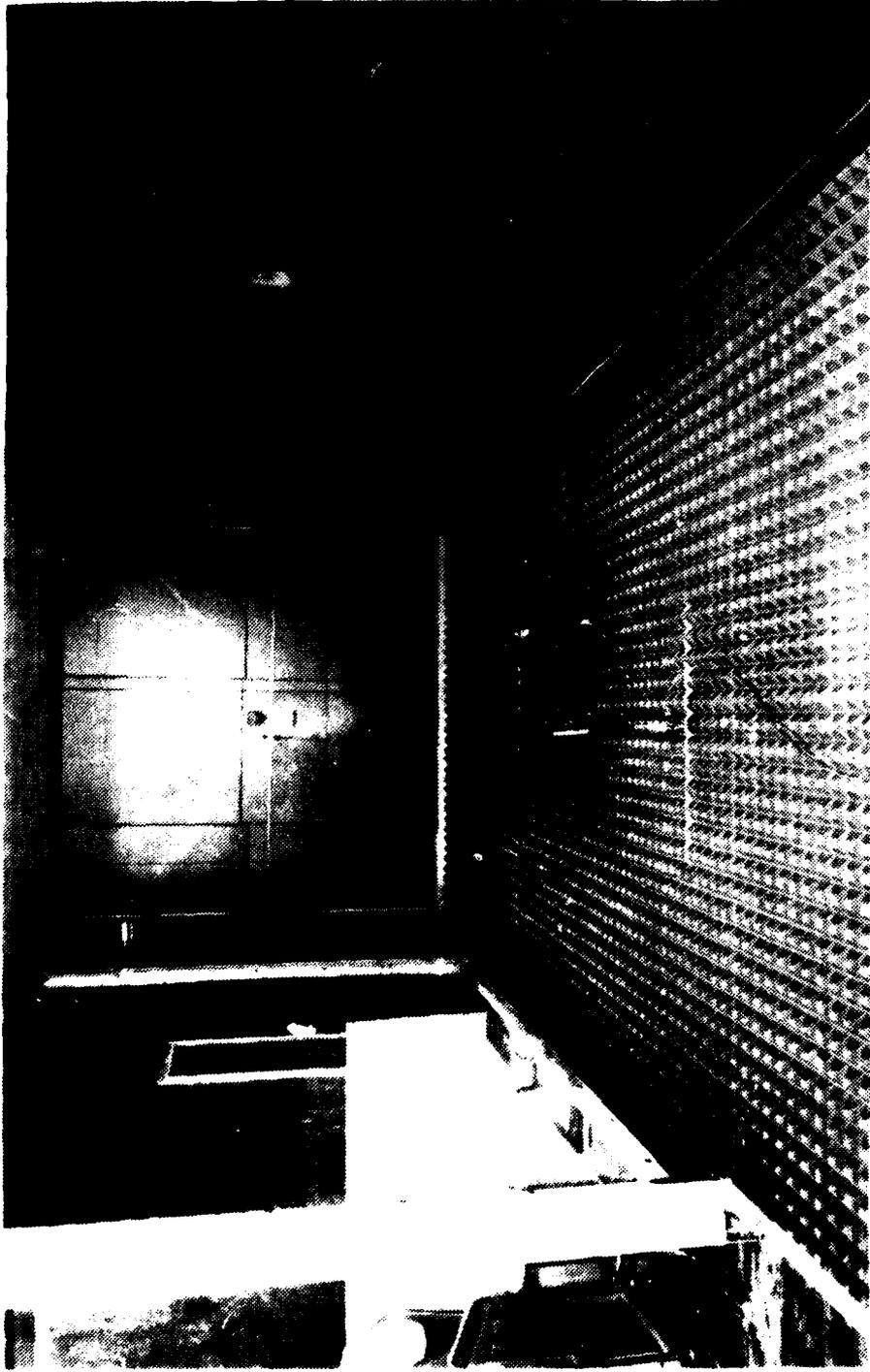
Figure 1

Low Speed Wind Tunnel and Roughness Elements
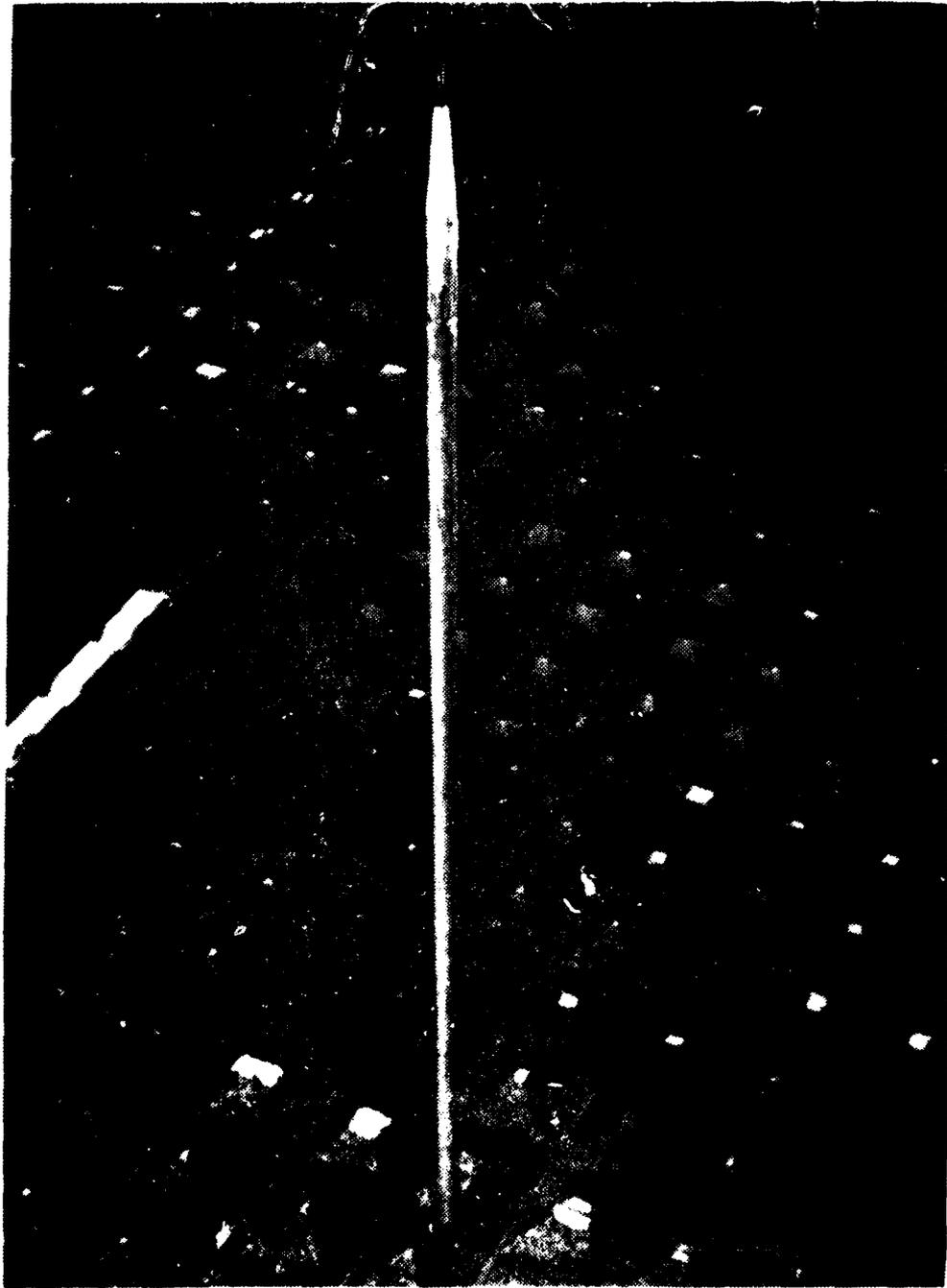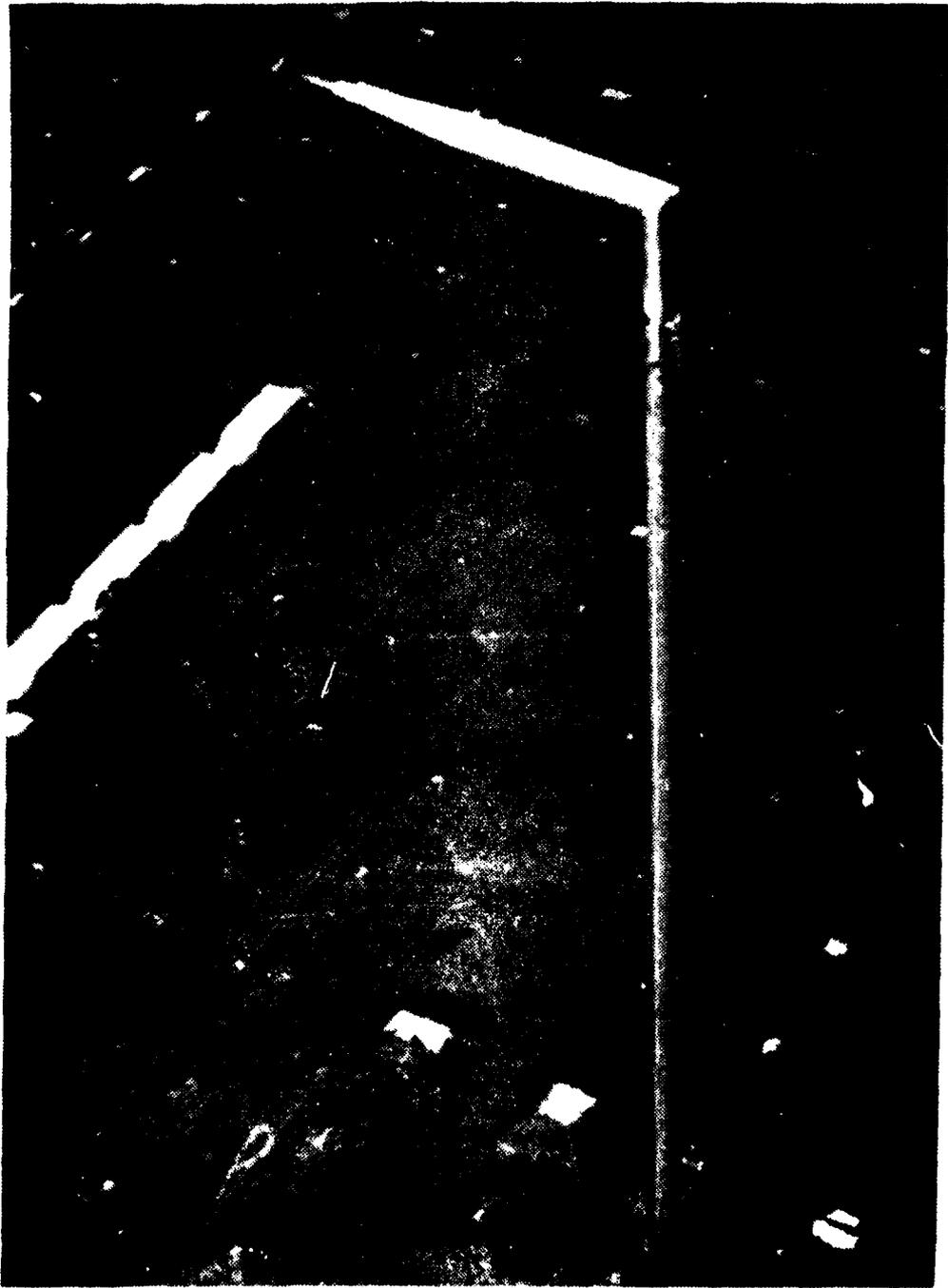
Figure 4

Anemometer and Correlator
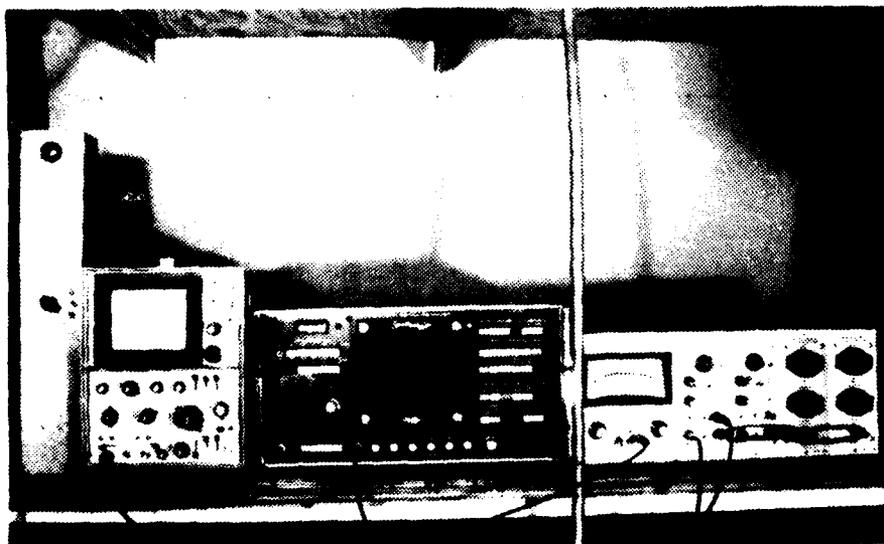
Figure 5

Frequency Counter
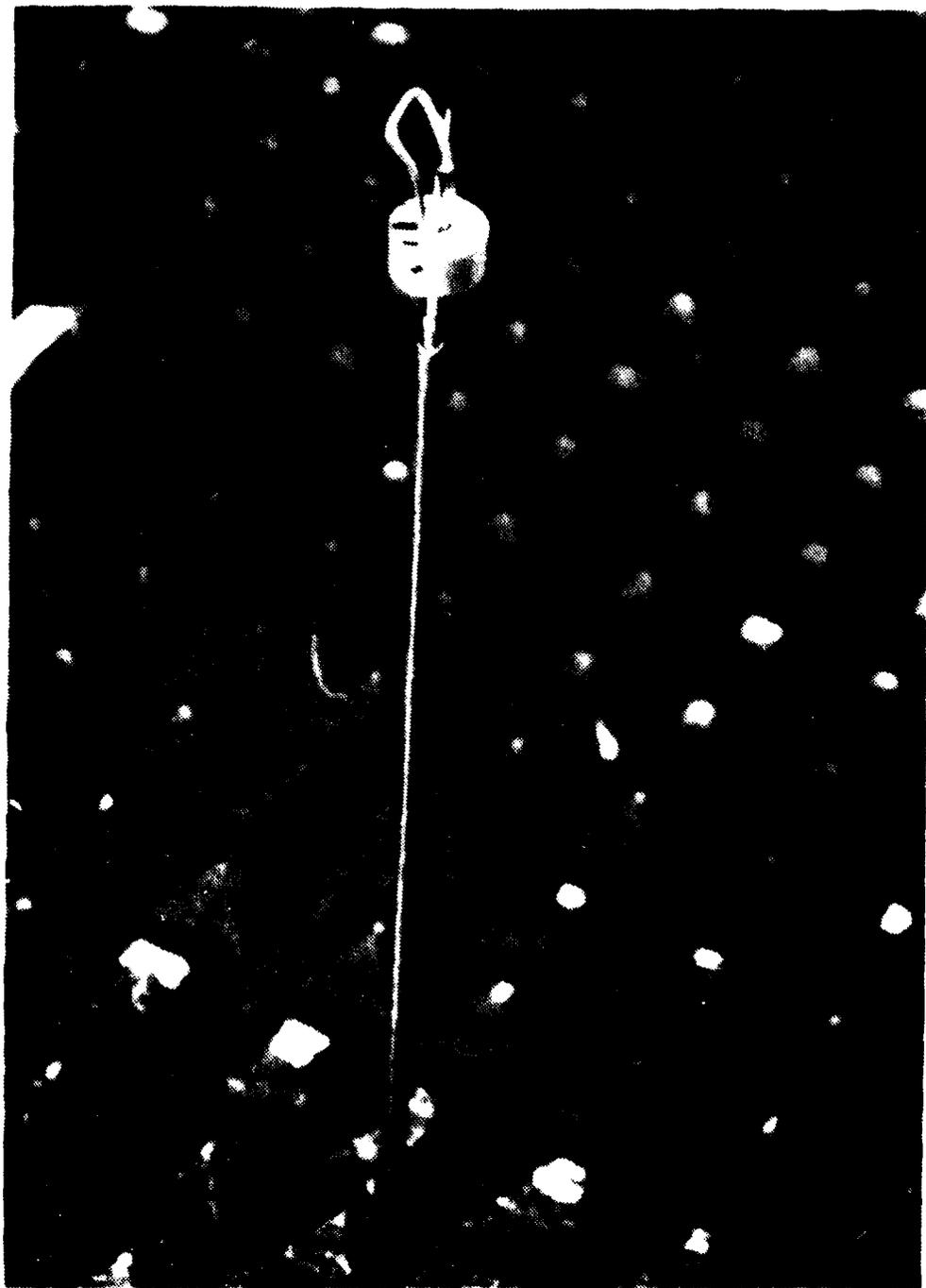
Figure 6
Velocimeter
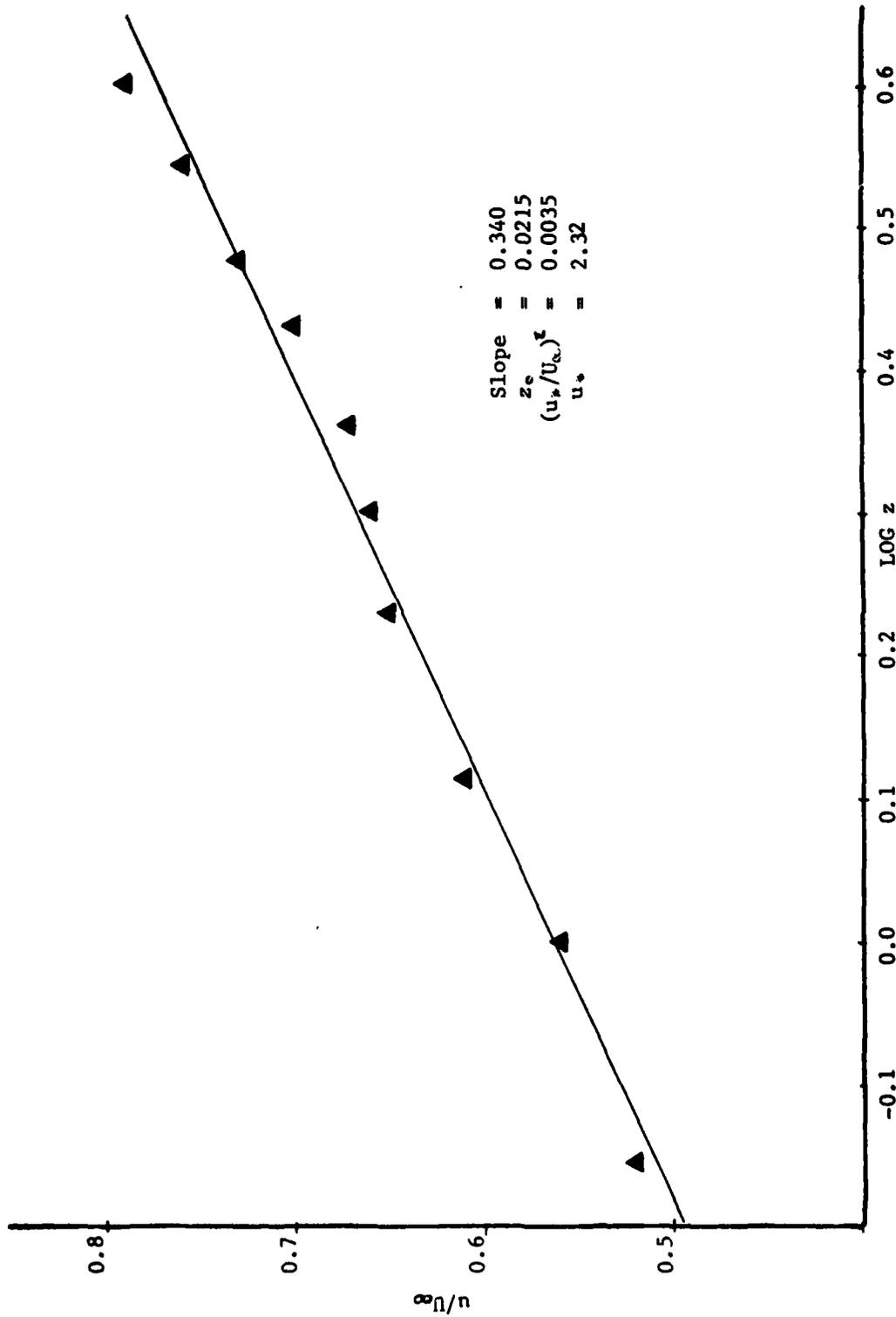
Figure 7

Velocity Profile at 72 inches Downwind

Slope = 0.375
z_0 = 0.0326
$(u_*/U_\infty)^2$ = 0.0043
u_* = 2.52

LOG z
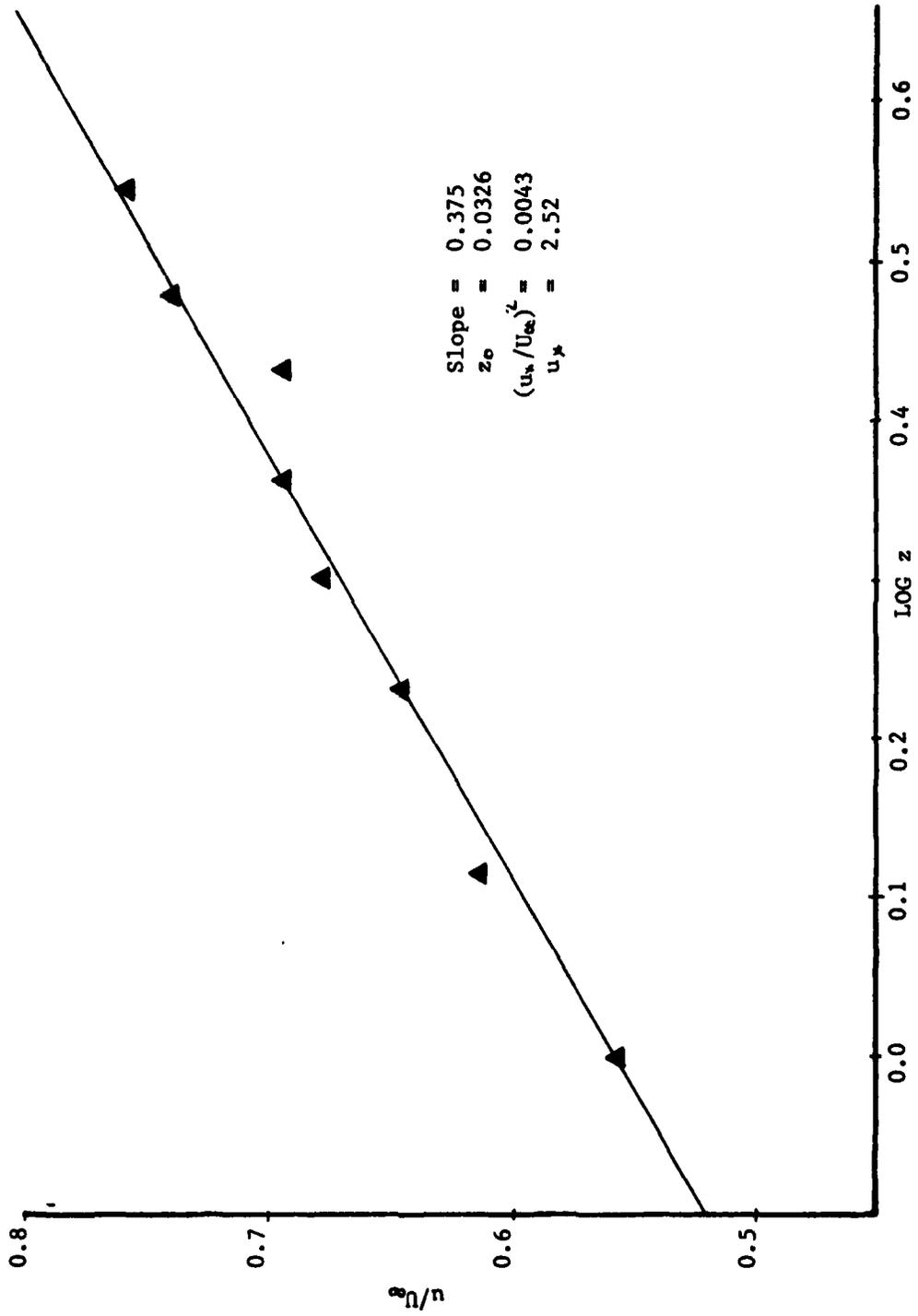
Figure 8

Velocity Profile at 109 inches Downwind

u/U_∞

35
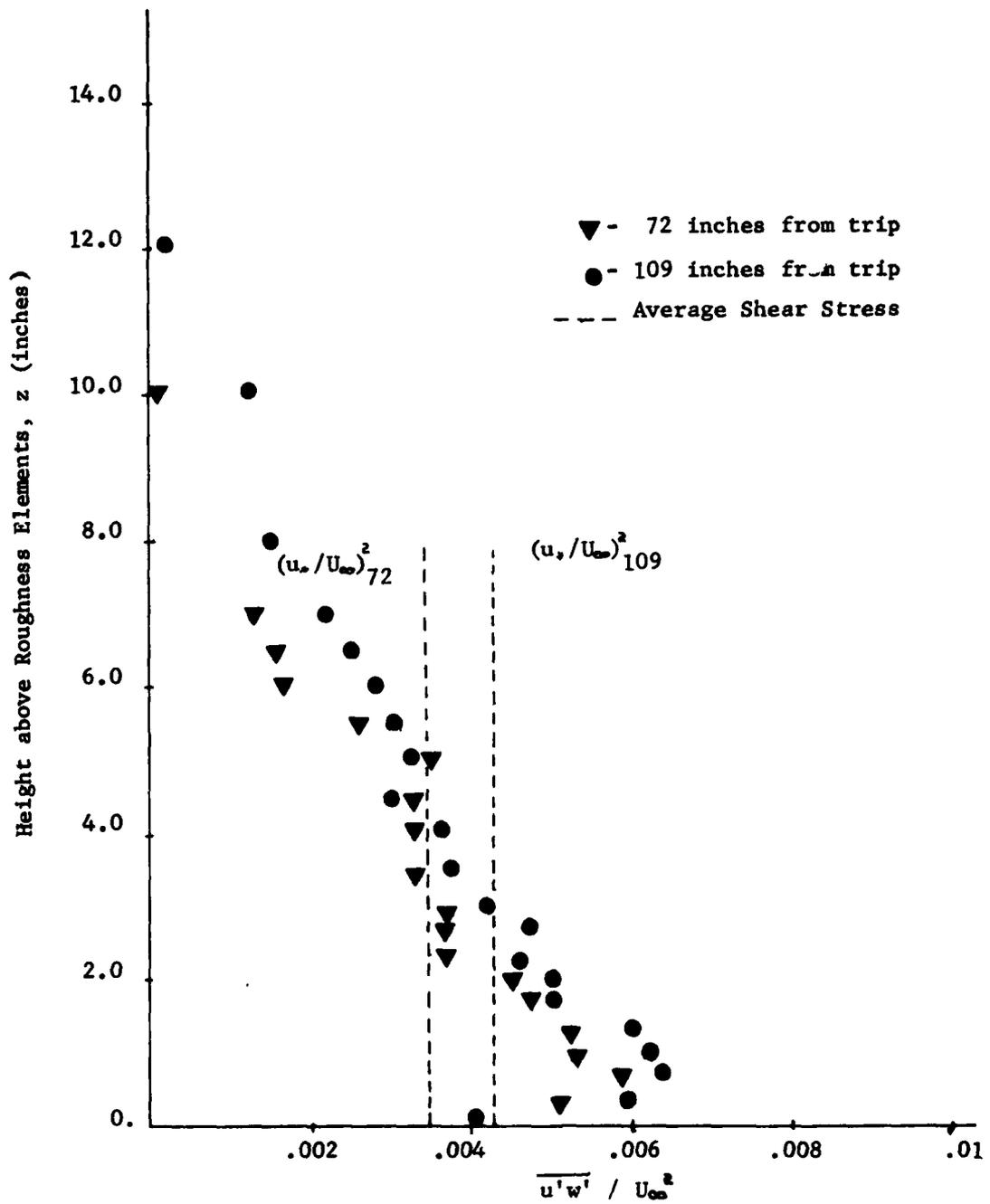
Figure 9
Vertical Distribution of Shear Stress at
72 and 109 inches Downwind

36
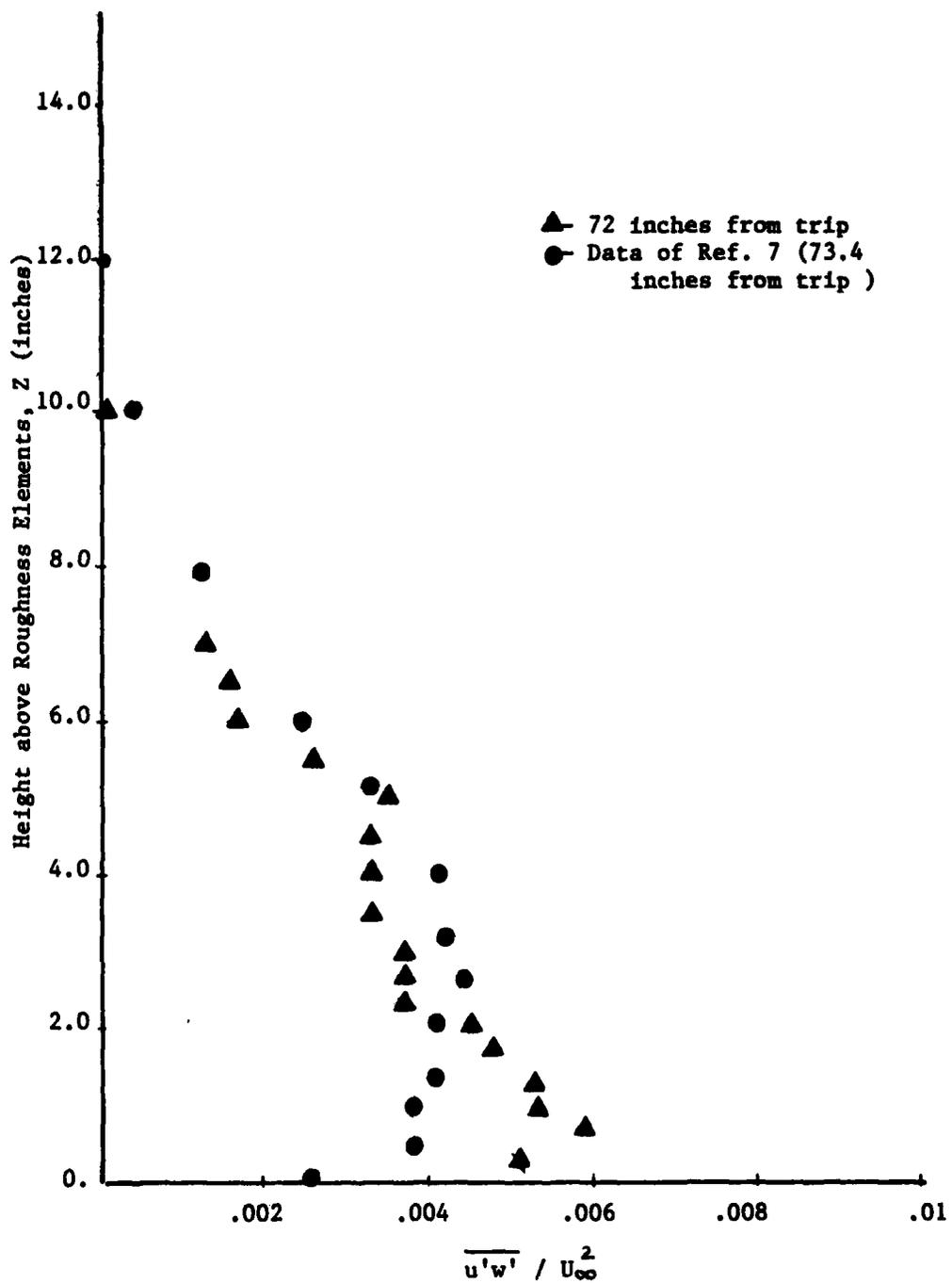
Figure 10
Vertical Distribution of Shear Stress at
72 inches Downwind Compared to the Data of Ref. 7
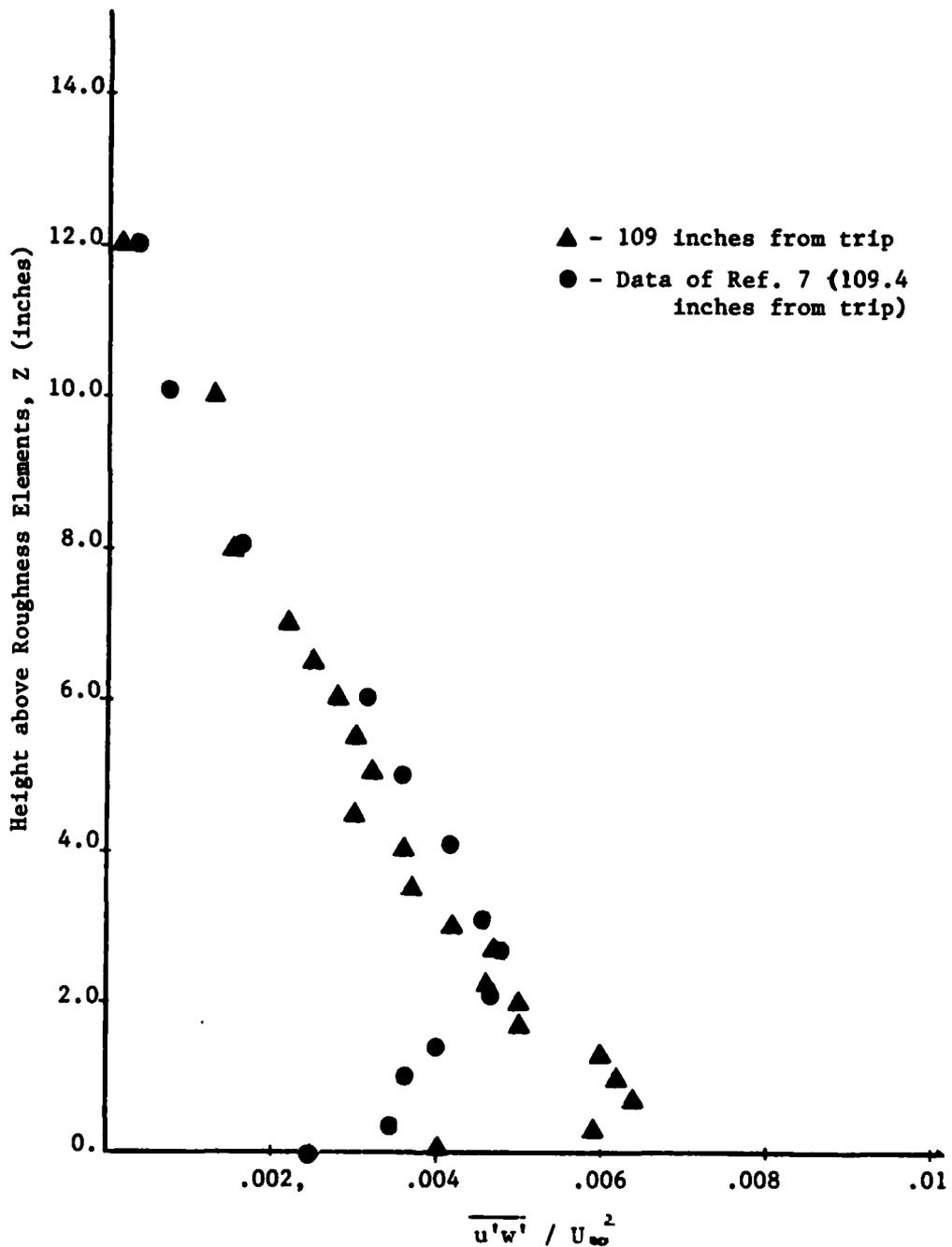
Figure 11
Vertical Distribution of Shear Stress at
109 inches Downwind Compared to the Data of Ref. 7
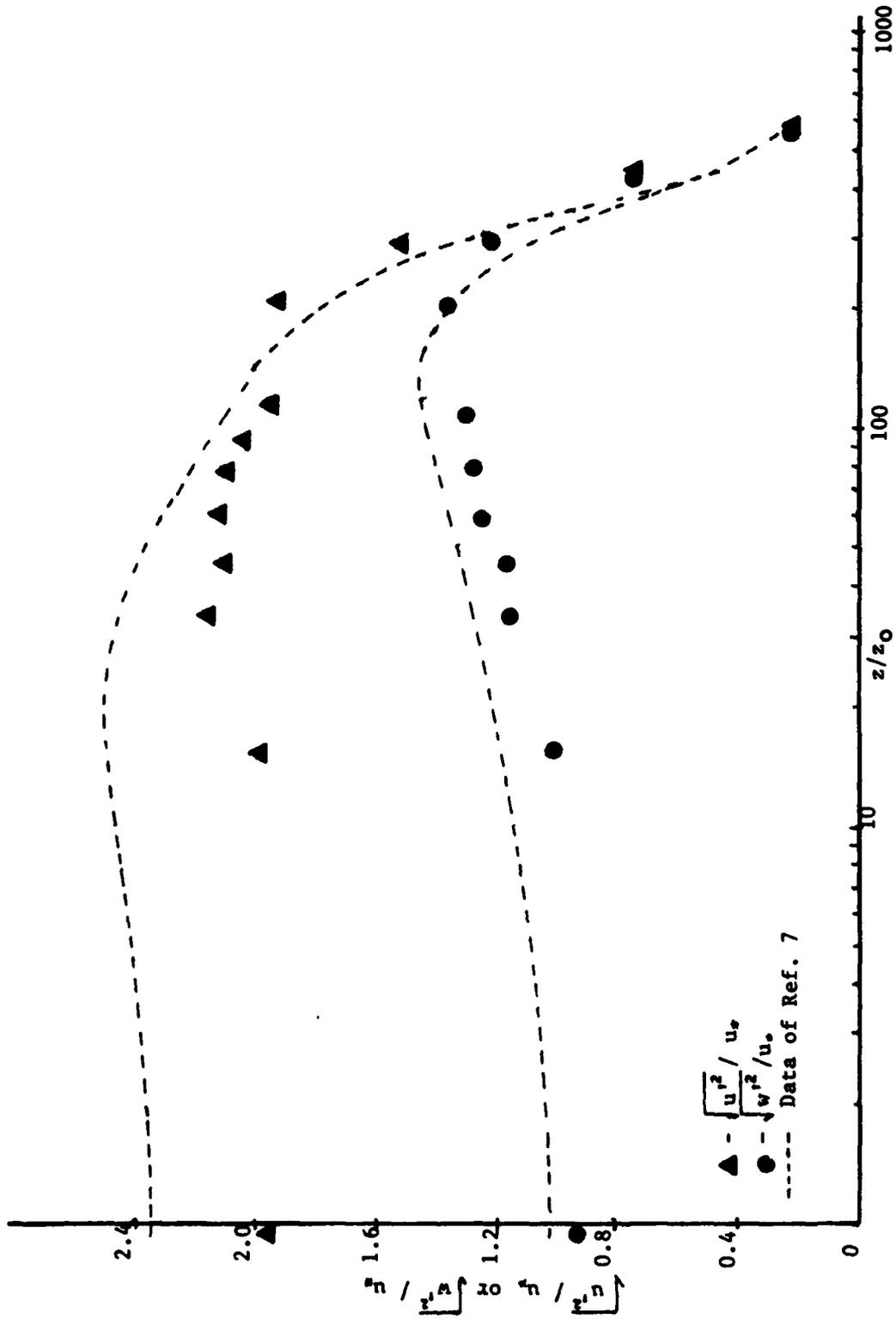
Figure 12
Comparison of Turbulence Intensities at
72 inches Downwind to the Data of Ref. 7

39
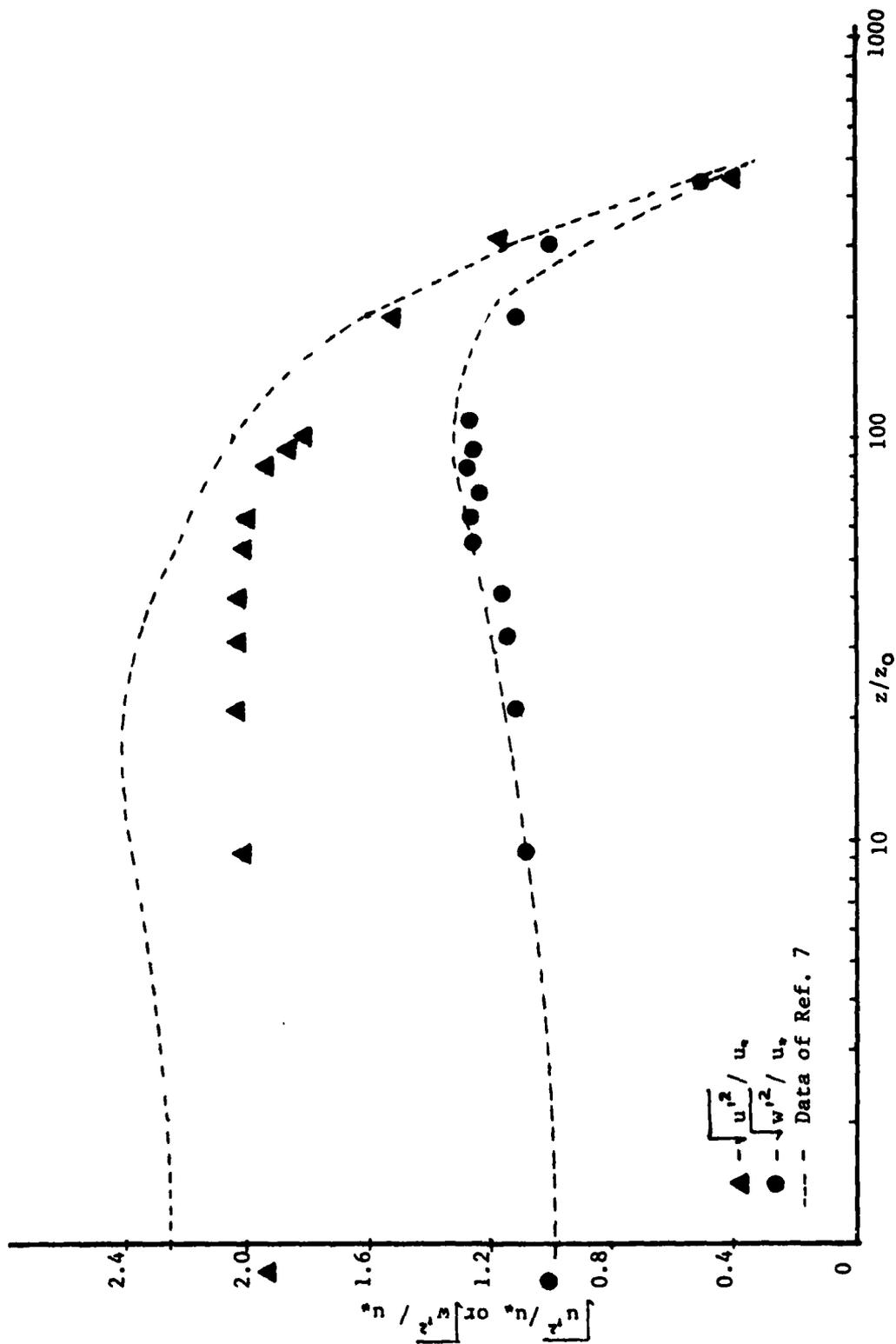
Figure 13
Comparison of Turbulence Intensities at
109 inches to the Data of Ref. 7

z/z_O

$\sqrt{u'^2}/u_*$ or $\sqrt{w'^2}/u_*$

$\sqrt{u'^2}/u_*$
$\sqrt{w'^2}/u_*$
Data of Ref. 7

40

Figure 14
Burner Can

41

Figure 15
Exhaust Nozzle and Thermocouple Probe
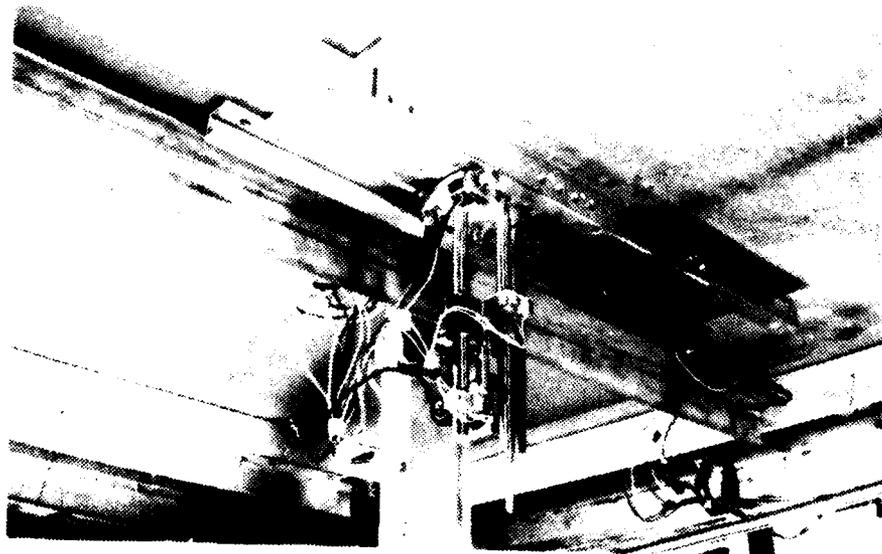
Figure 16
Thermocouple Traverse System
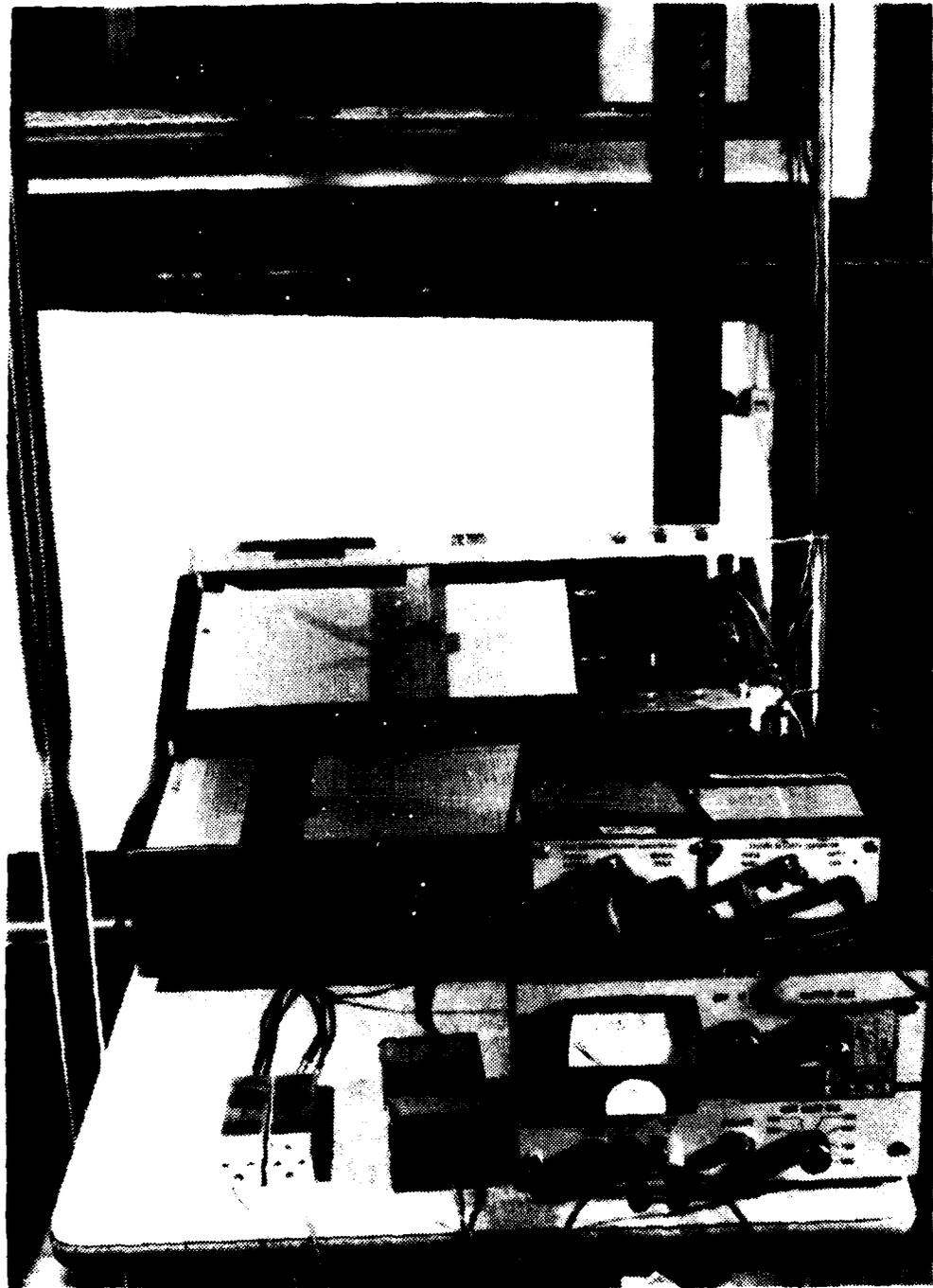
Figure 17
X-Y Plotters for Temperature Measuring
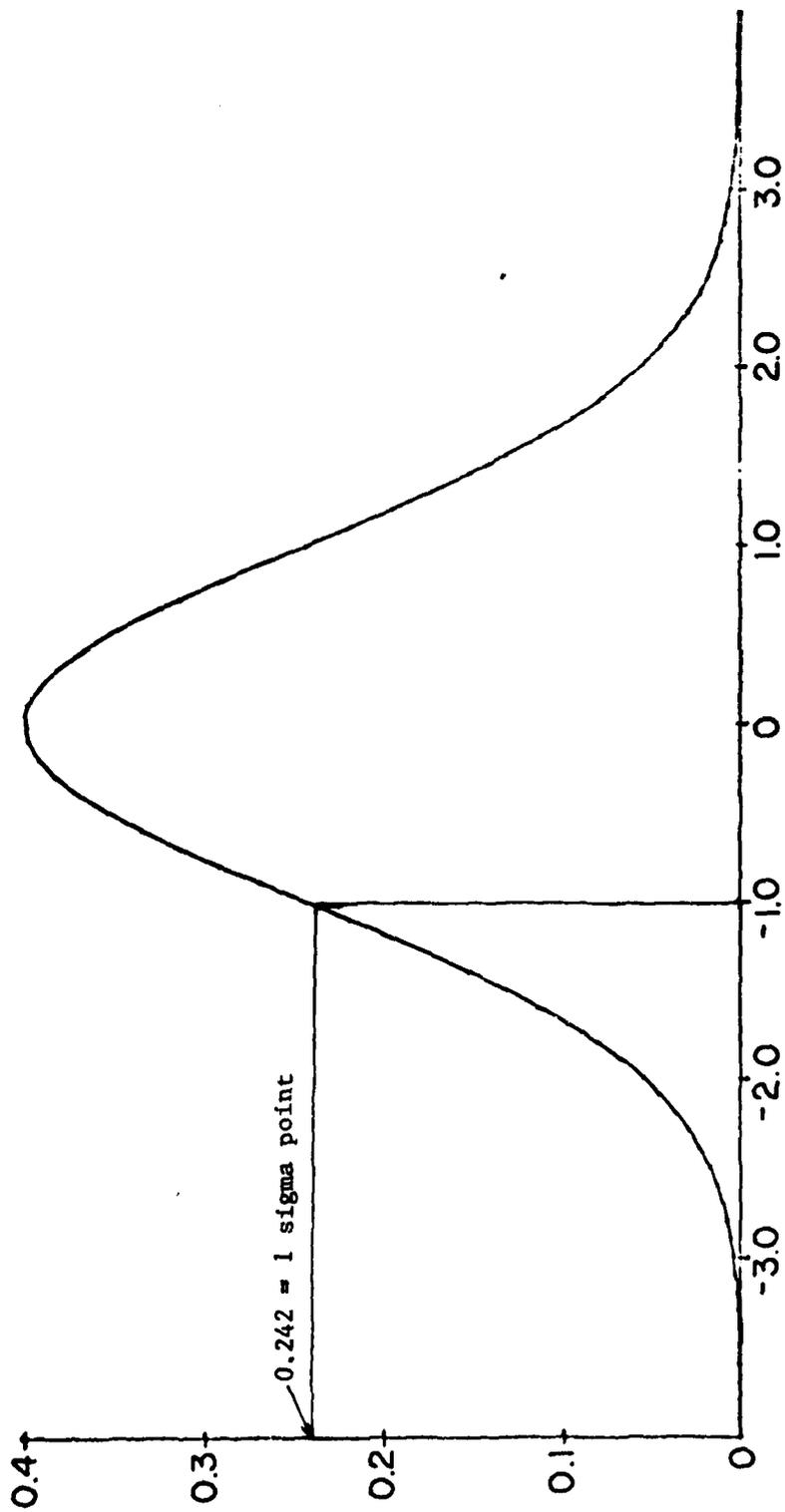
Figure 18

Standard Normal Distribution

44
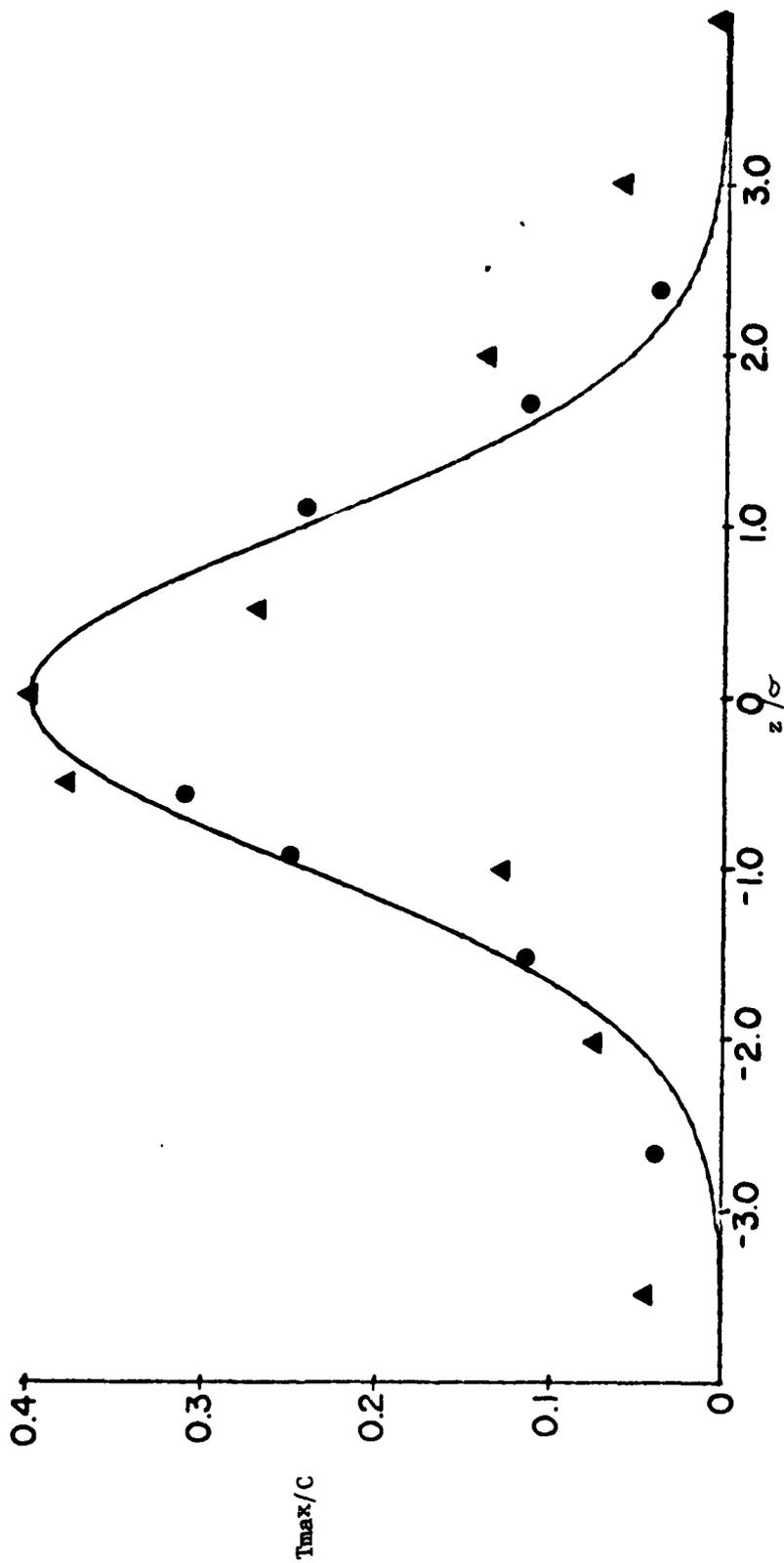
Figure 19

Comparison of Vertical Distribution of
Temperature to a Standard Normal Distribution
for Zero Degrees Angle of Incidence

45

Figure 20
Comparison of Vertical Distribution of
Temperature to a Standard Normal Distribution
for Zero Degrees Angle of Incidence

Downwind Distance
▲ - 86.2 JD
● - 51.7 JD
■ - 120.6 JD

z/σ

T_{max}/C

0.4
0.3
0.2
0.1
0

-3.0 -2.0 -1.0 0 1.0 2.0 3.0
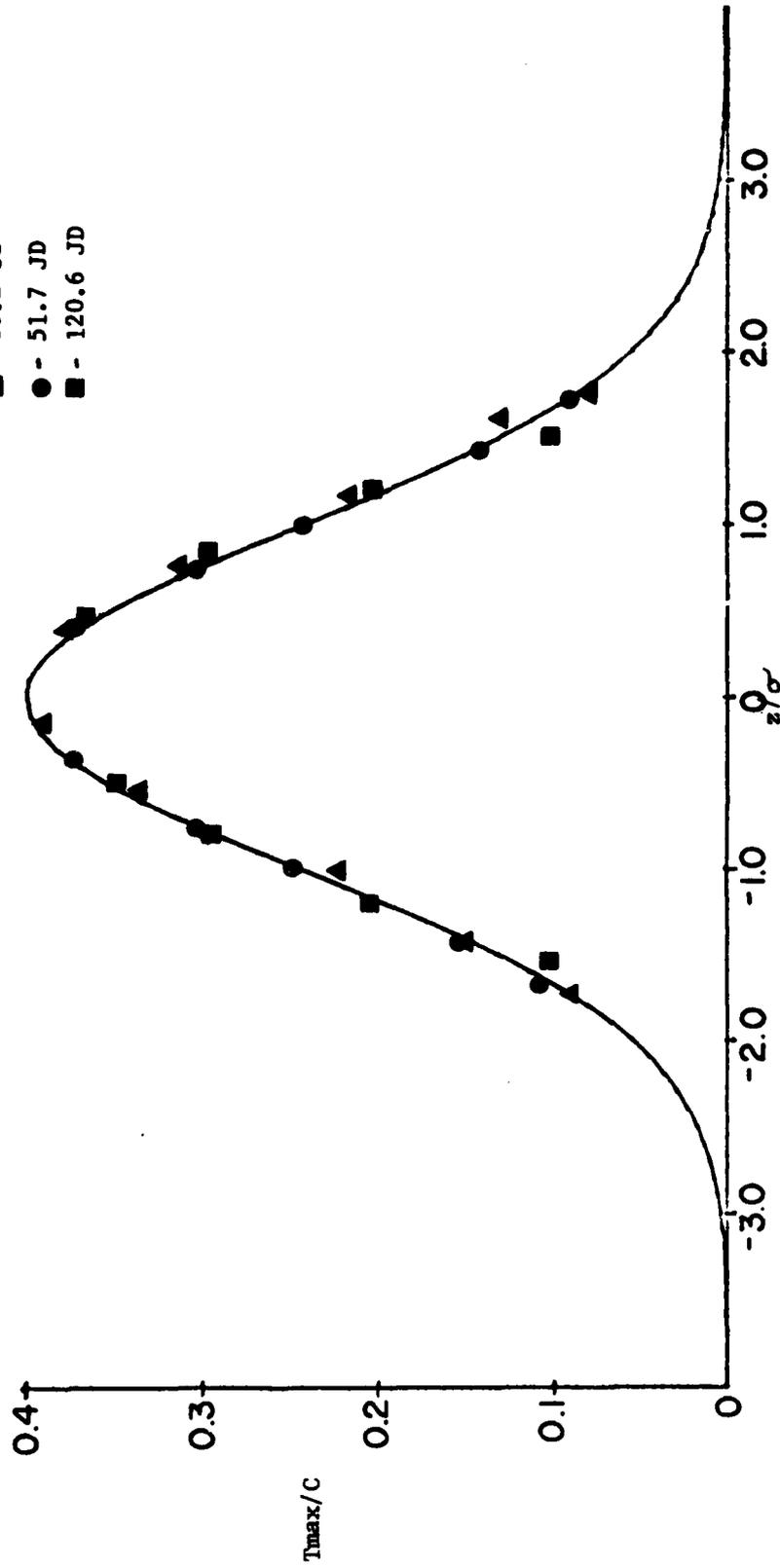
Figure 21
Comparison of Vertical Distribution of
Temperature to a Standard Normal Distribution
for Zero Degrees Angle of Incidence

47
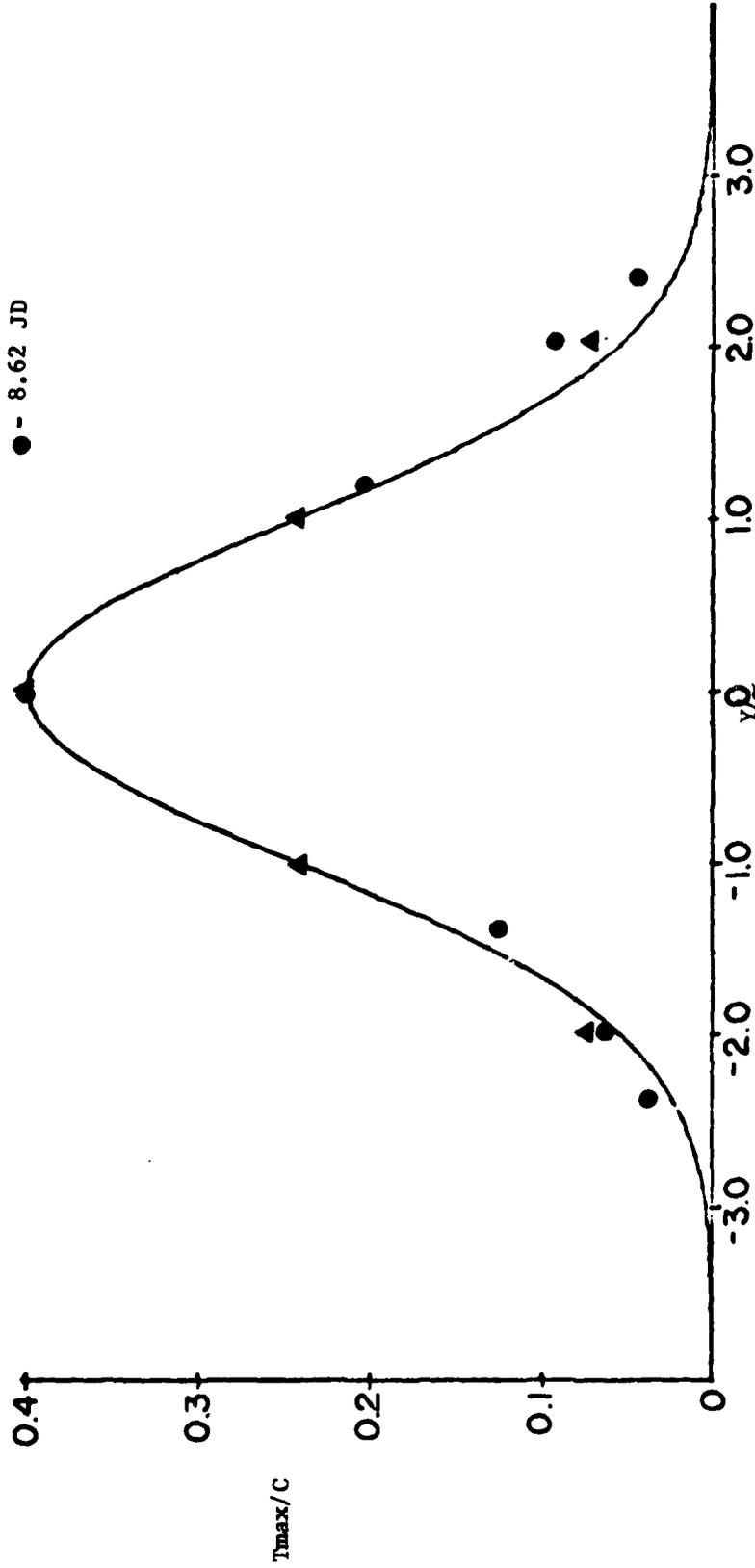
Figure 22

Comparison of Horizontal Distribution of
Temperature to a Standard Normal Distribution
for Zero Angle of Incidence

48
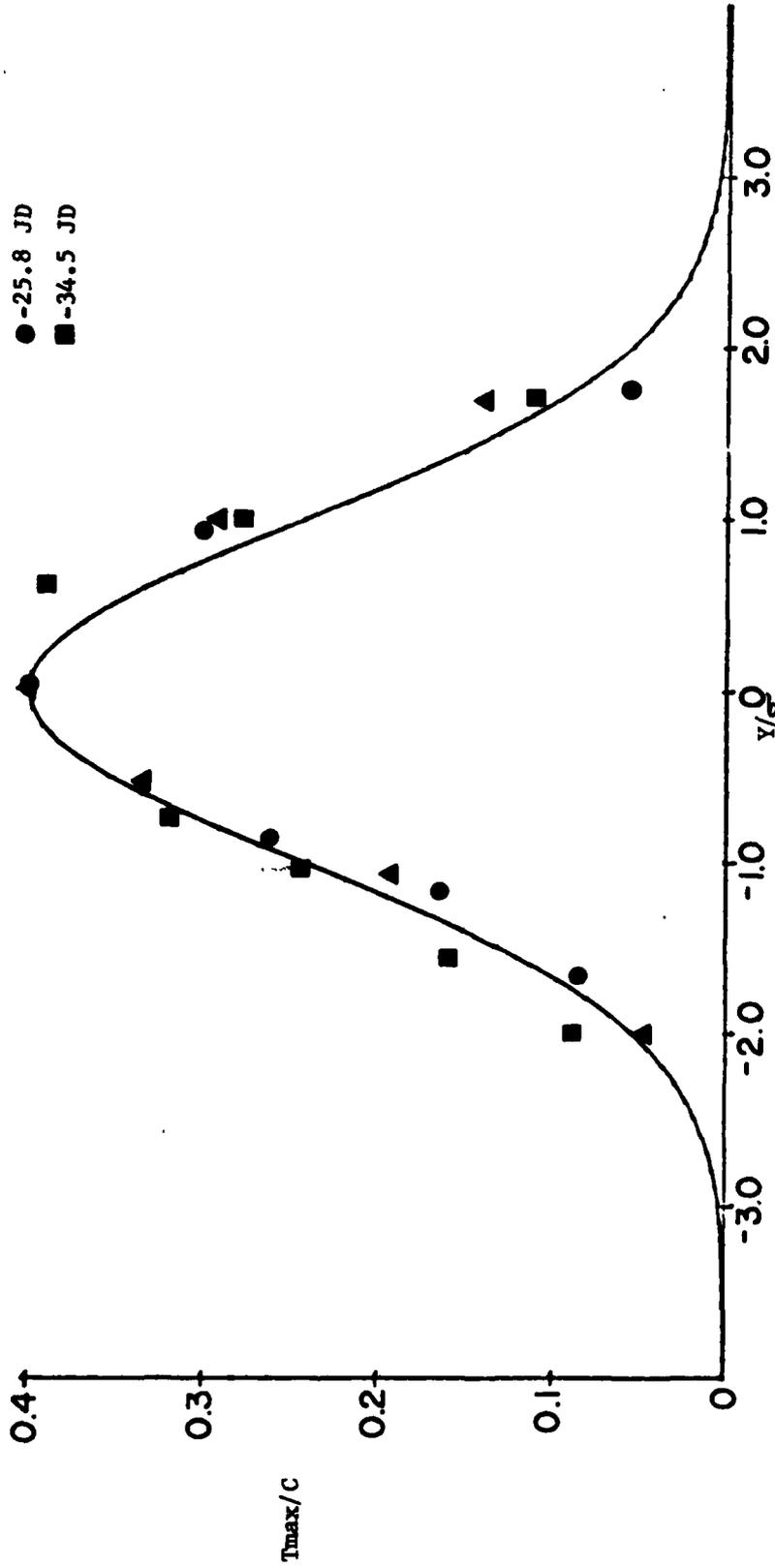
Figure 23

Comparison of Horizontal Distribution of
Temperature to a Standard Normal Distribution
for Zero Angle of Incidence

Figure 24

Comparison of Horizontal Distribution of
Temperature to a Standard Normal Distribution
for Zero Angle of Incidence

Angles of Incidence
▲ - 29 Degrees
● - 45 Degrees
■ - 67 Degrees
▽ - 90 Degrees
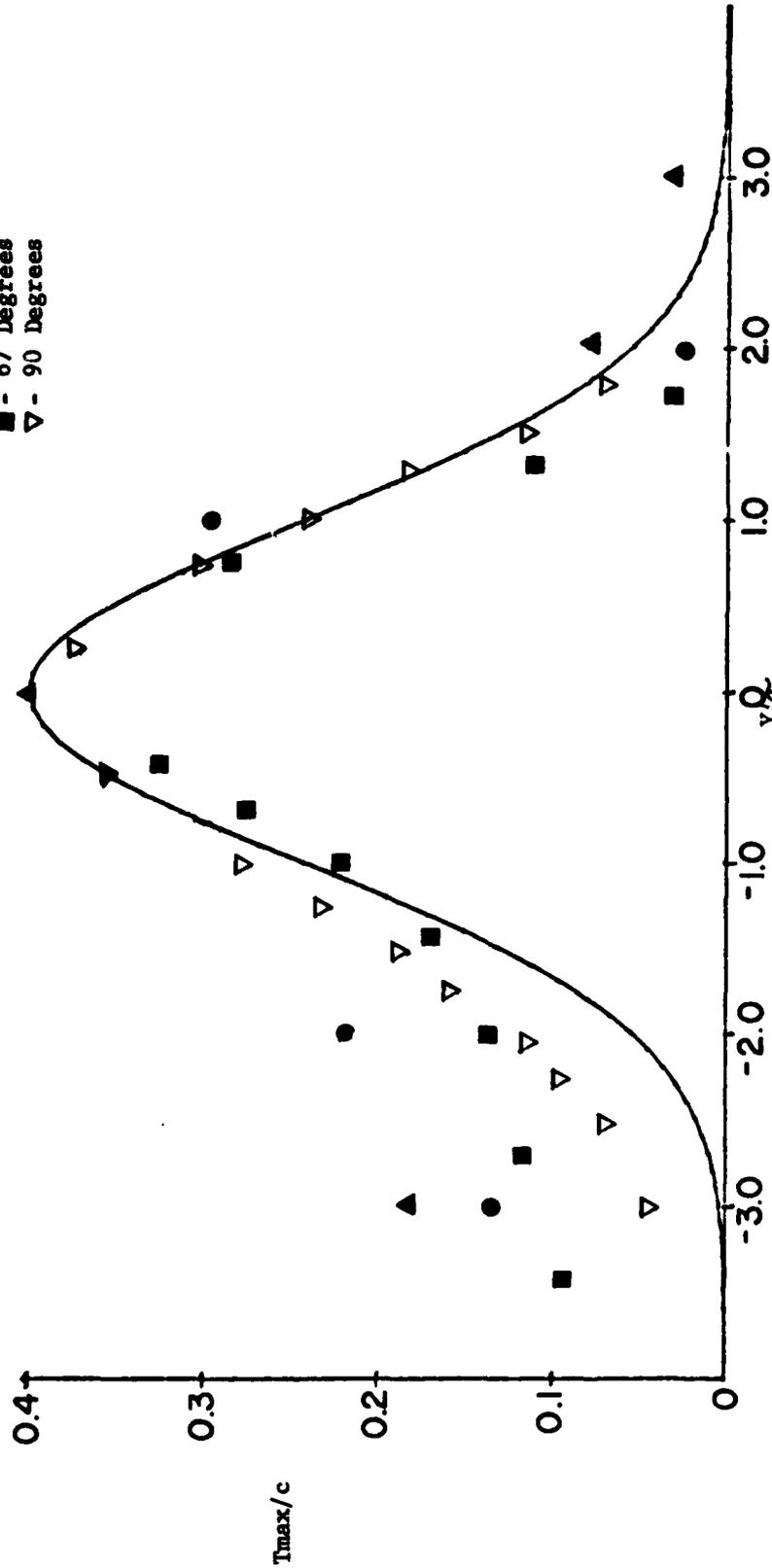
Figure 25

Comparison of Horizontal Distribution of Temperature to a
Standard Normal Distribution for Angles of Incidence at
1.72 Jet Diameters Downwind from the Nozzle

51

Figure 26

Comparison of Horizontal Distribution of Temperature to a
Standard Normal Distribution for Angles of Incidence at
8.62 Jet Diameters Downwind from the Nozzle

Angles of Incidence
▲ – 29 Degrees
● – 45 Degrees
■ – 67 Degrees
▽ – 90 Degrees
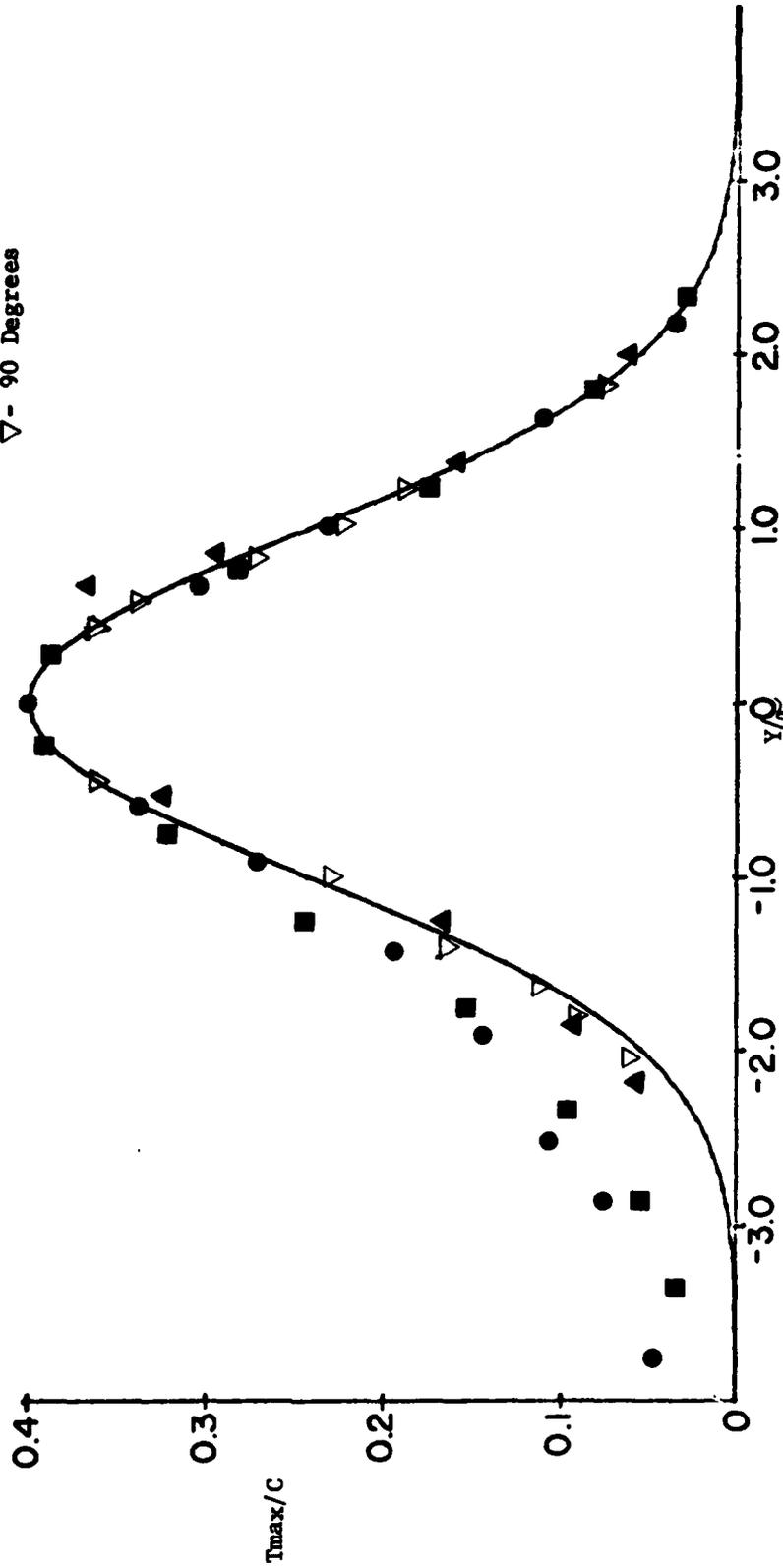
Figure 27

Comparison of Horizontal Distribution of Temperature to a
Standard Normal Distribution for Angles of Incidence at
17.2 Jet Diameters Downwind from the Nozzle

53
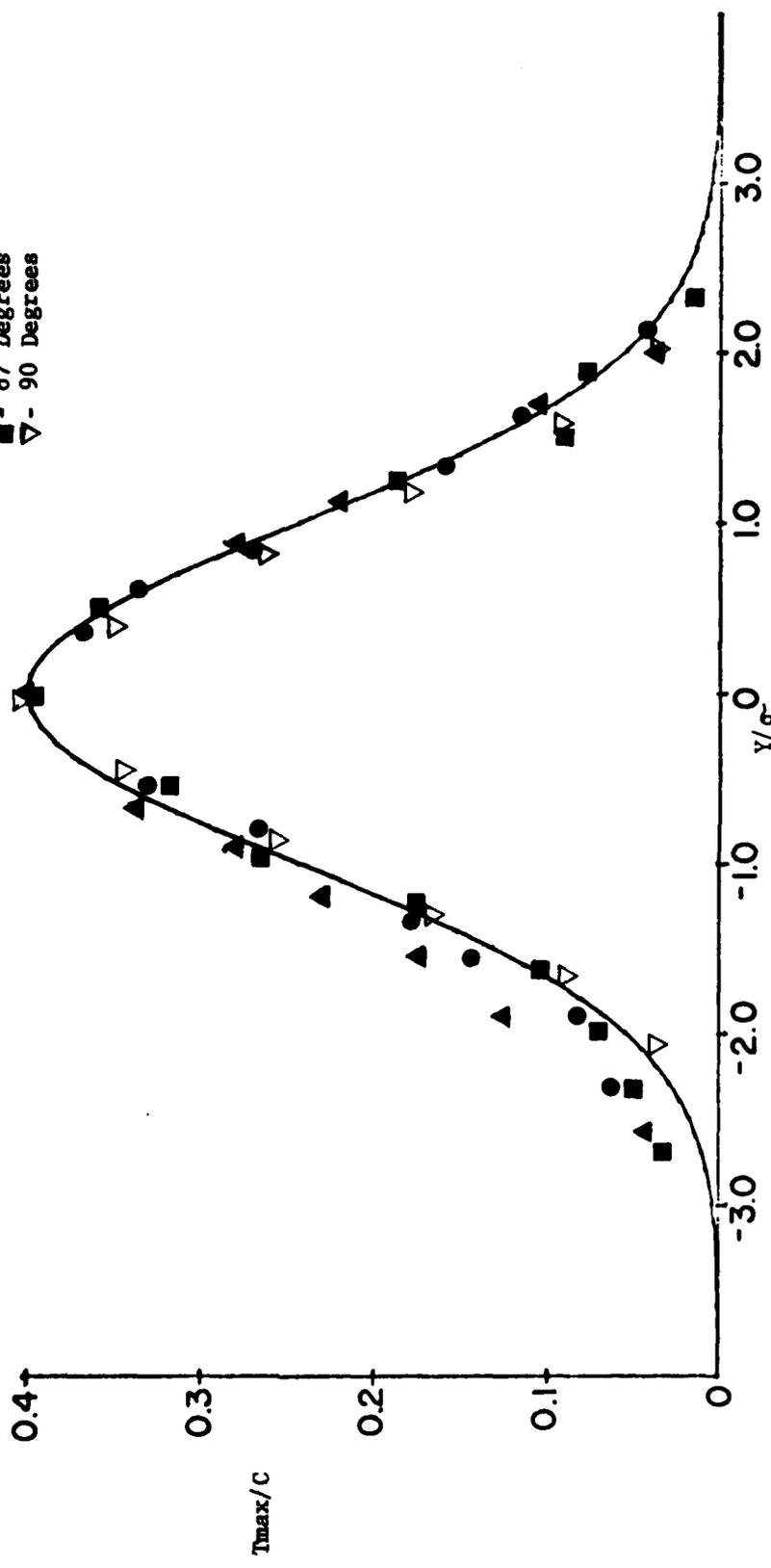
Figure 28

Comparison of Horizontal Distribution of Temperature to a
Standard Normal Distribution for Angles of Incidence at
25.8 Jet Diameters Downwind from the Nozzle

54
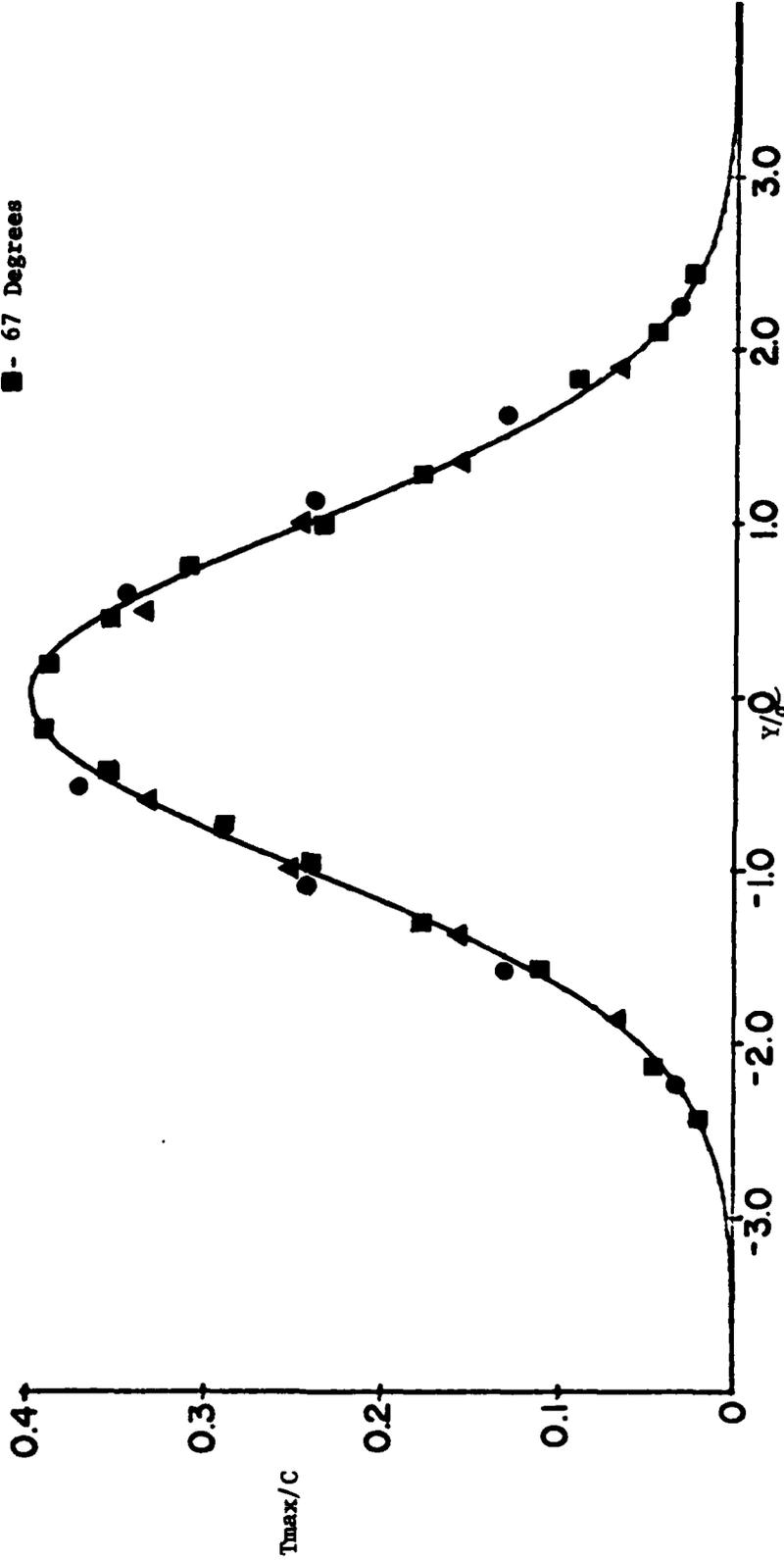
Figure 29

Comparison of Horizontal Distribution of Temperature to a
Standard Normal Distribution for Angles of Incidence at
34.5 Jet Diameteres from the Nozzle

Figure 30

Comparison of Horizontal Distribution of Temperature to a
Standard Normal Distribution for Angles of Incidence at
51.7 Jet Diameters from the Nozzle

Figure 31

Comparison of Horizontal Distribution of Temperature to a
Standard Normal Distribution for Angles of Incidence at
86.2 Jet Diameters Downwind from the Nozzle

Figure 32

Comparison of Horizontal Distribution of Temperature to a
Standard Normal Distribution for Angles of Incidence at
120.6 Jet Diameters Downwind from the Nozzle
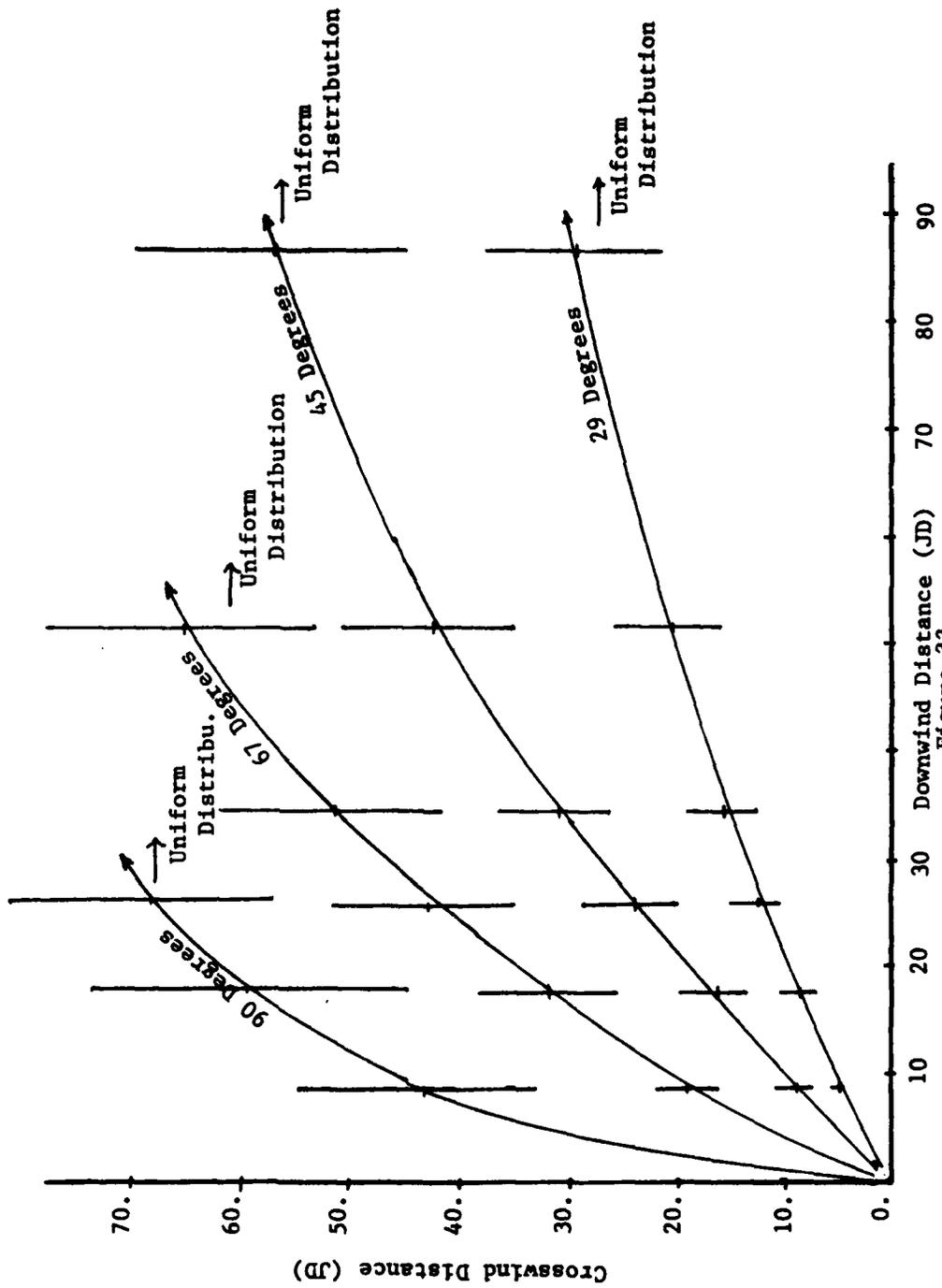
Spatial Representation of Plume Width as a Function of
Downwind and Horizontal Distances from the end of the
Nozzle for Different Angles of Incidence to the Wind

Figure 33

59
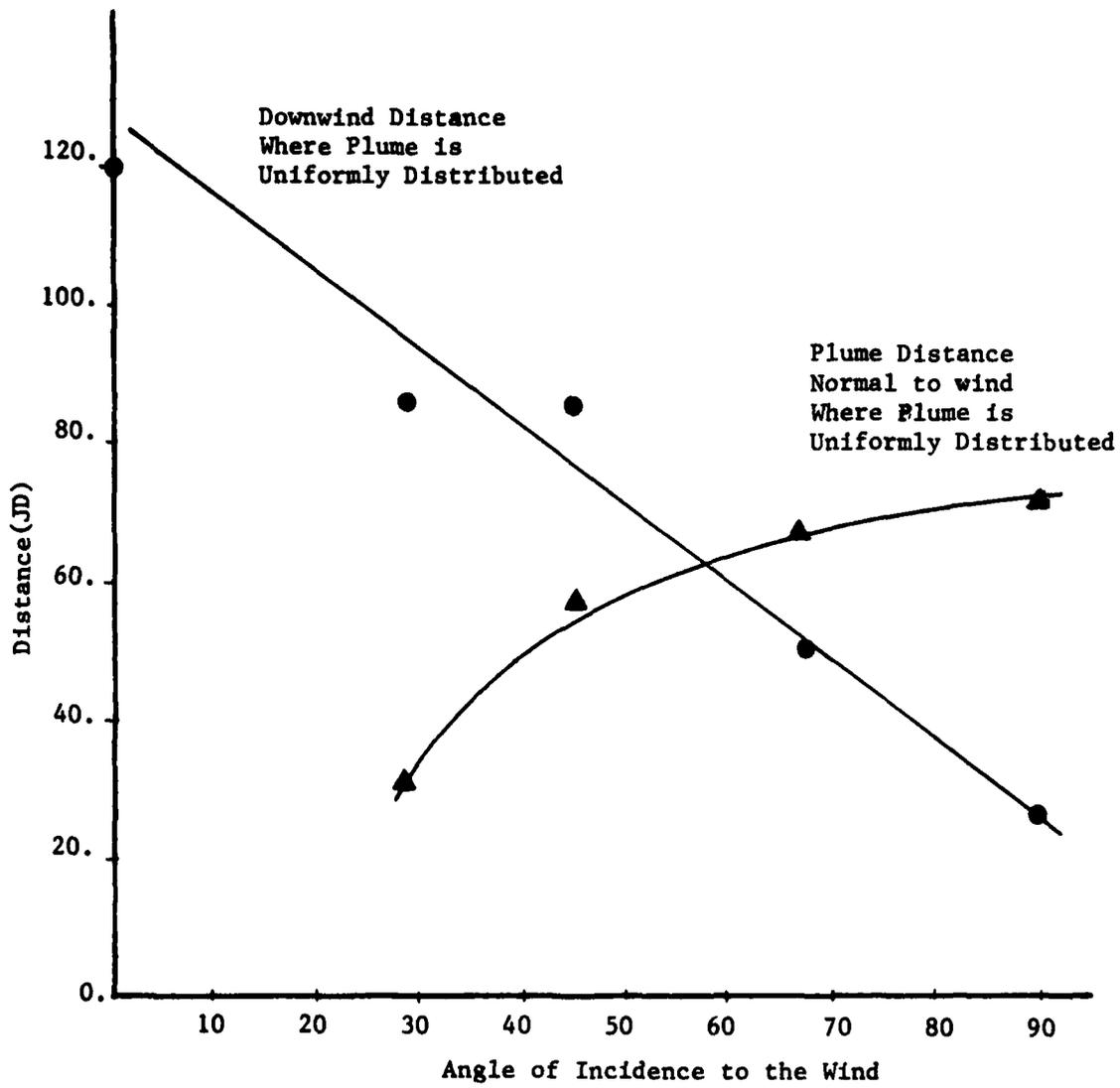
Figure 34

Distance Downwind and Normal to Wind from the Nozzle
Where the Plume is Uniformly Distributed

60
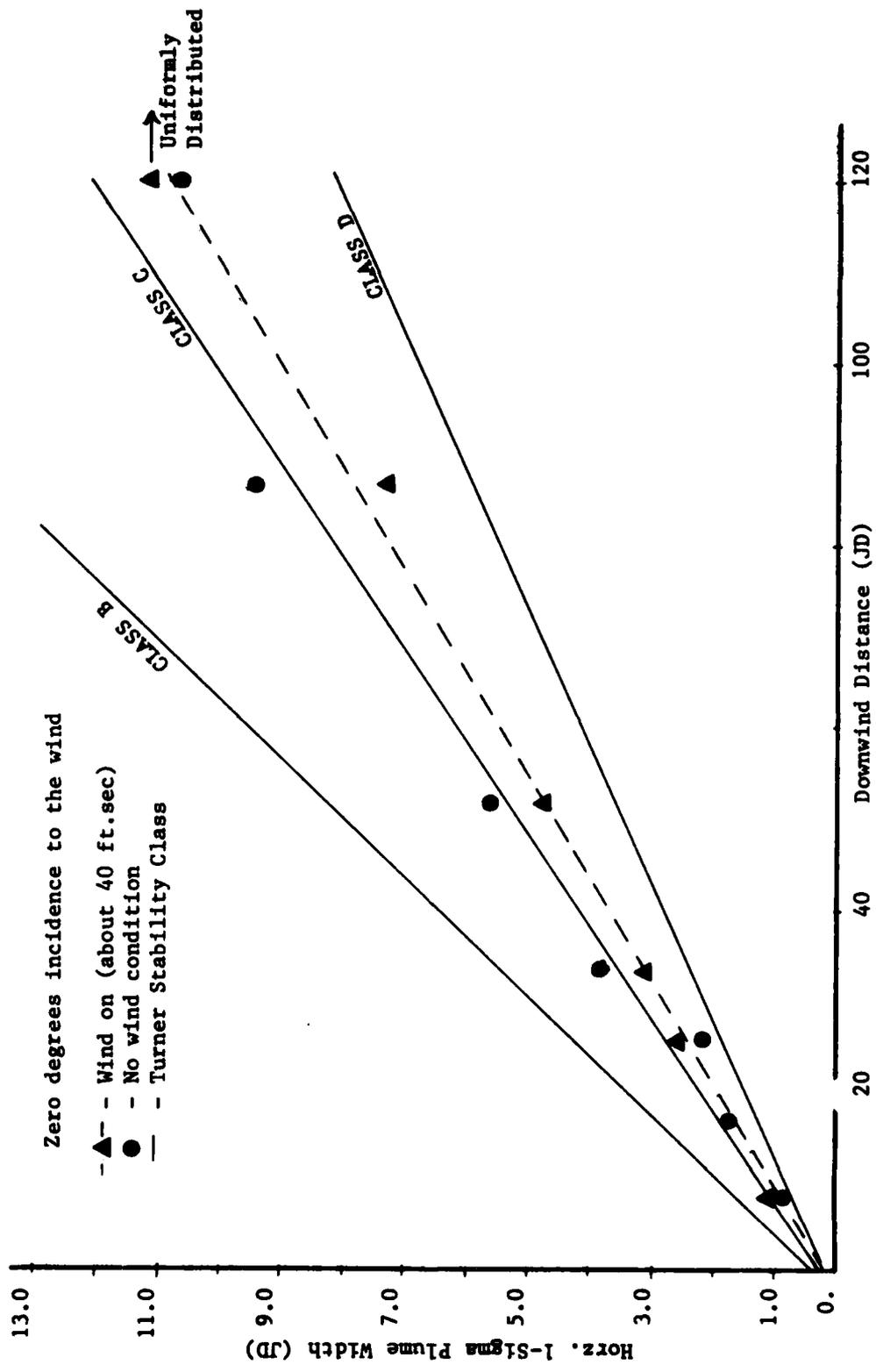
Figure 35

Horizontal Plume Width vs. Downwind Distance
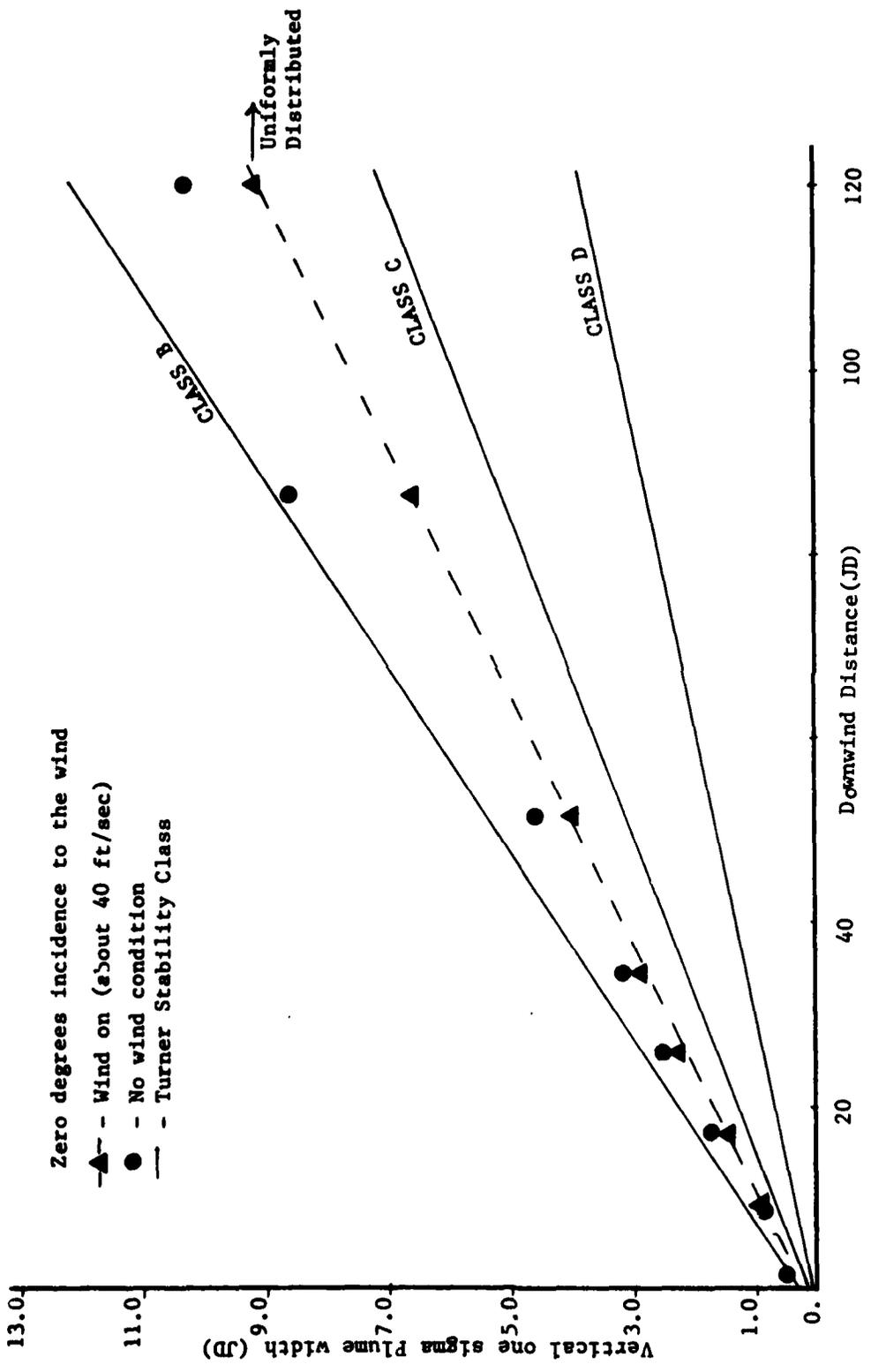
Figure 36

Vertical Plume Width vs. Downwind Distance
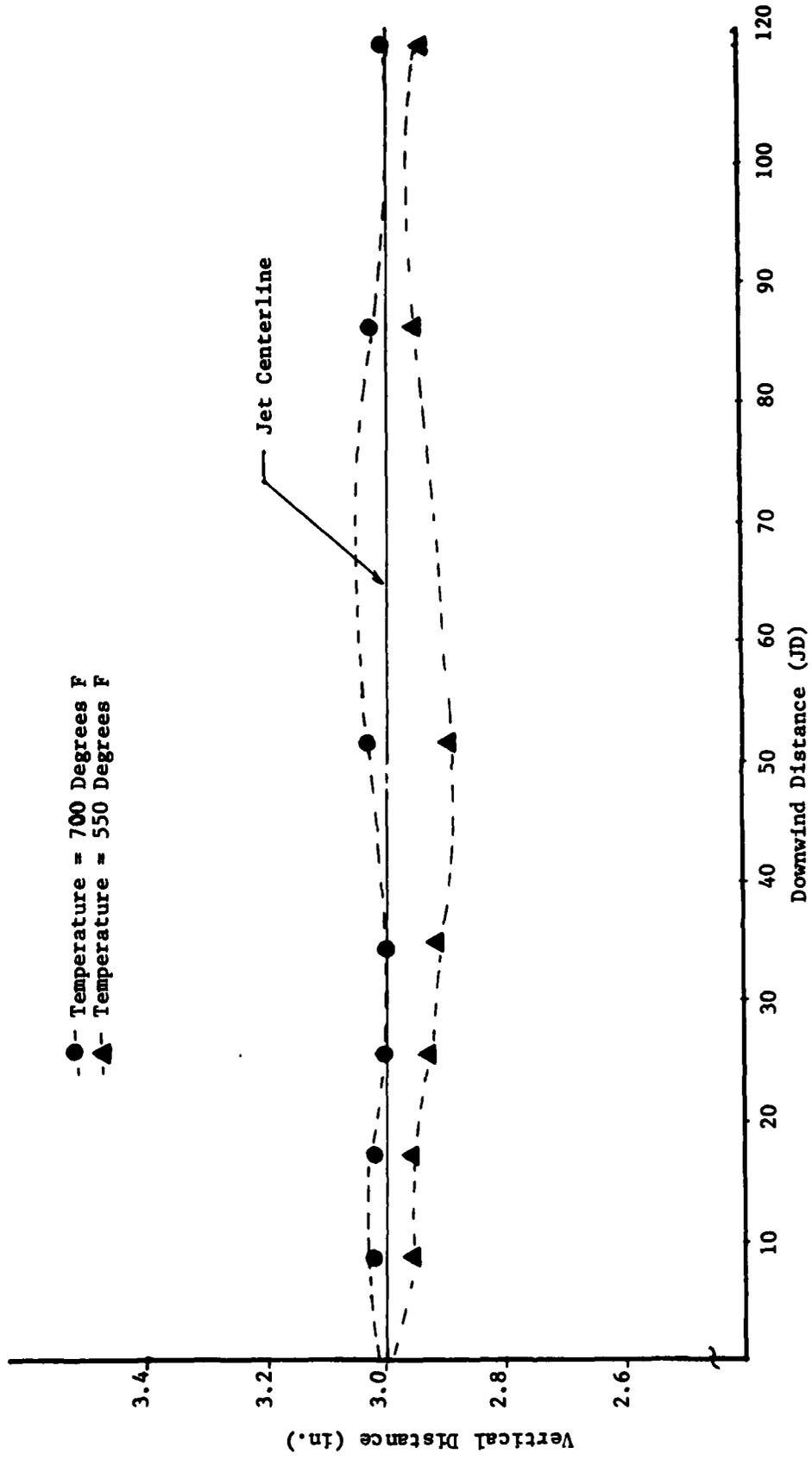
Figure 37

Plume Rise vs. Downwind Distance

-●- Temperature = 700 Degrees F
-▲- Temperature = 550 Degrees F

Jet Centerline

Downwind Distance (JD)

Vertical Distance (In.)

63
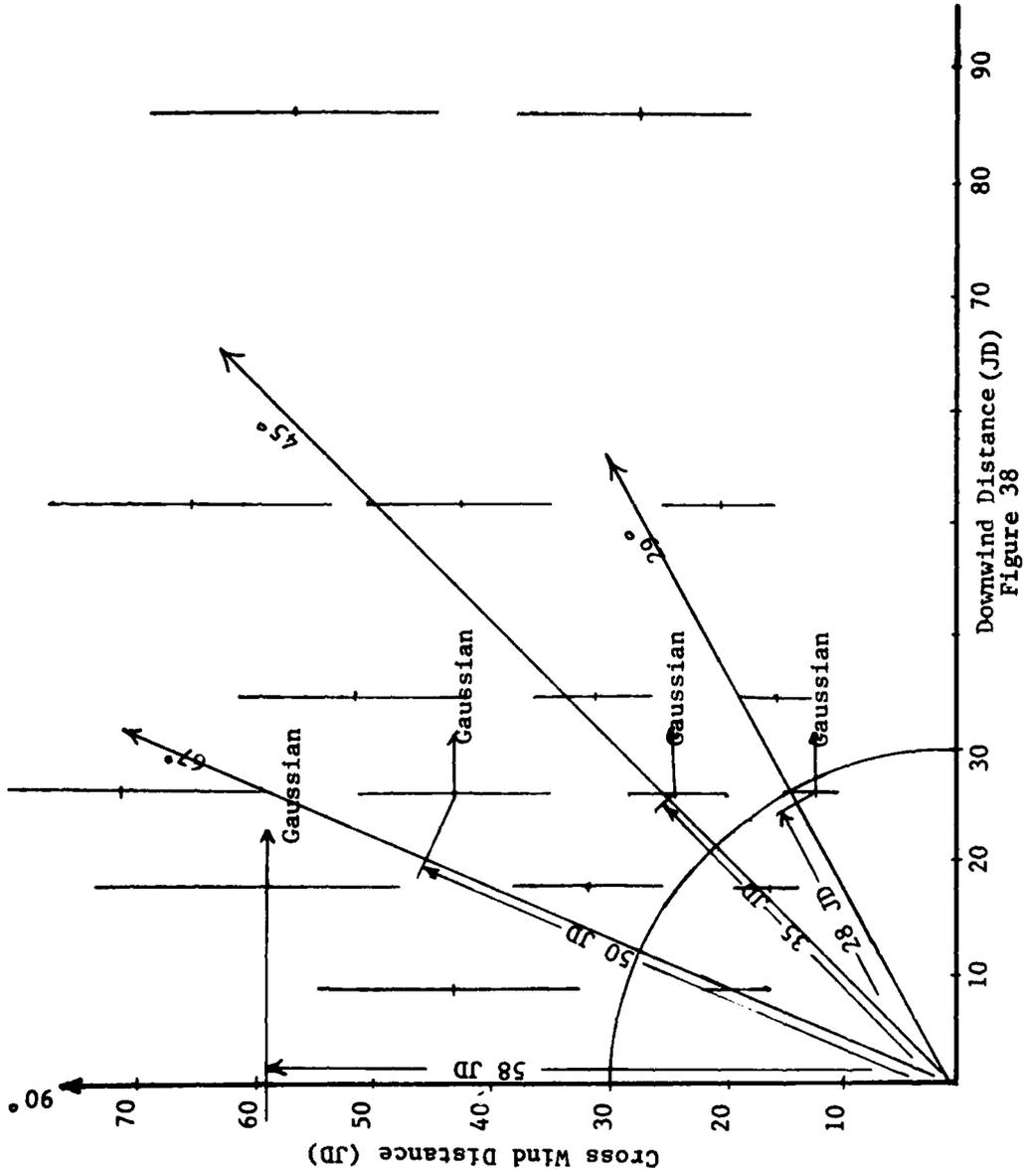
Jet Penetration vs. Downwind and Horizontal Distance from
the Nozzle for Different Angles of Incidence to the Wind

64
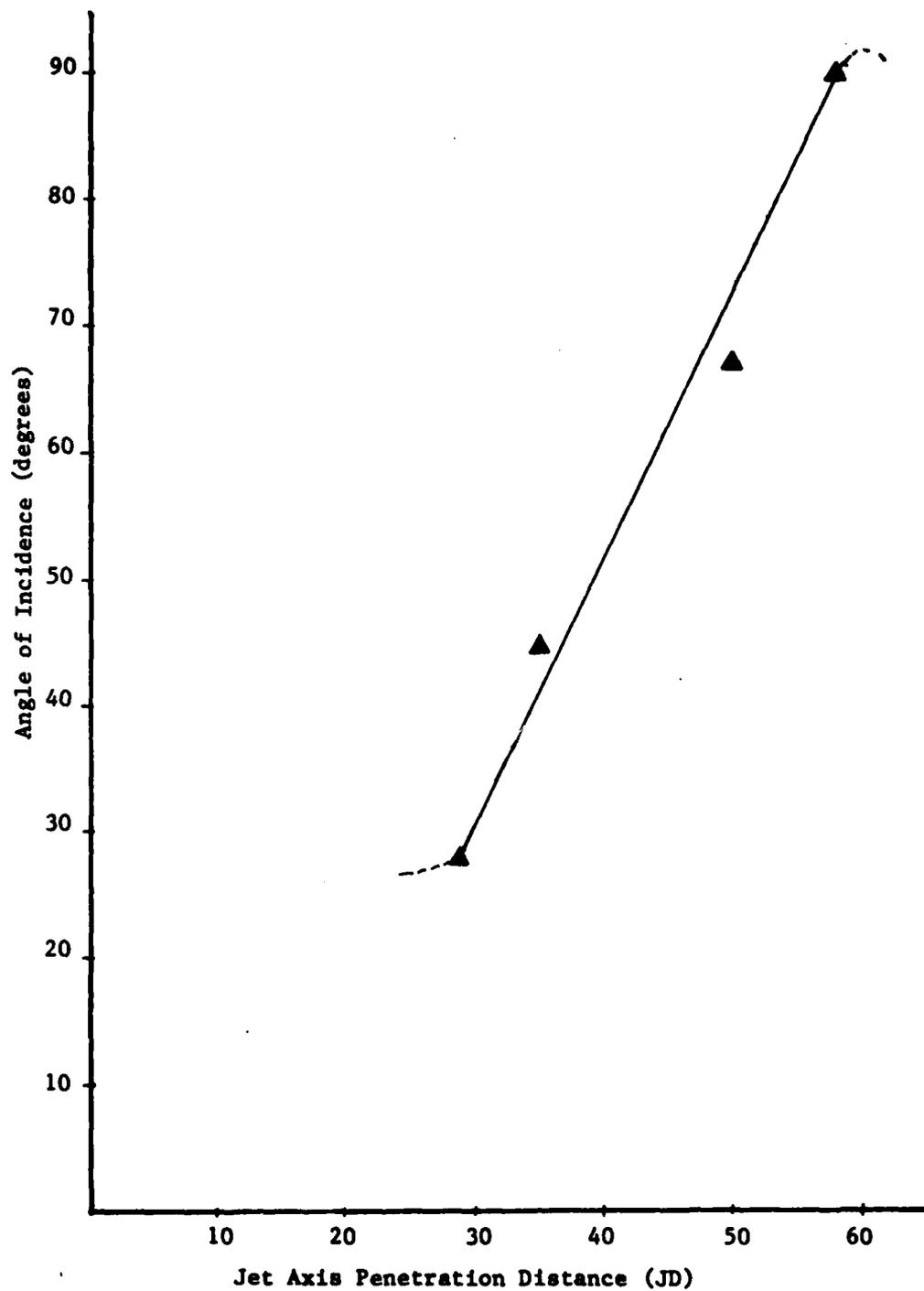
Figure 39

Jet Penetration Distance along the Jet
Axis vs. Angle of Incidence

65
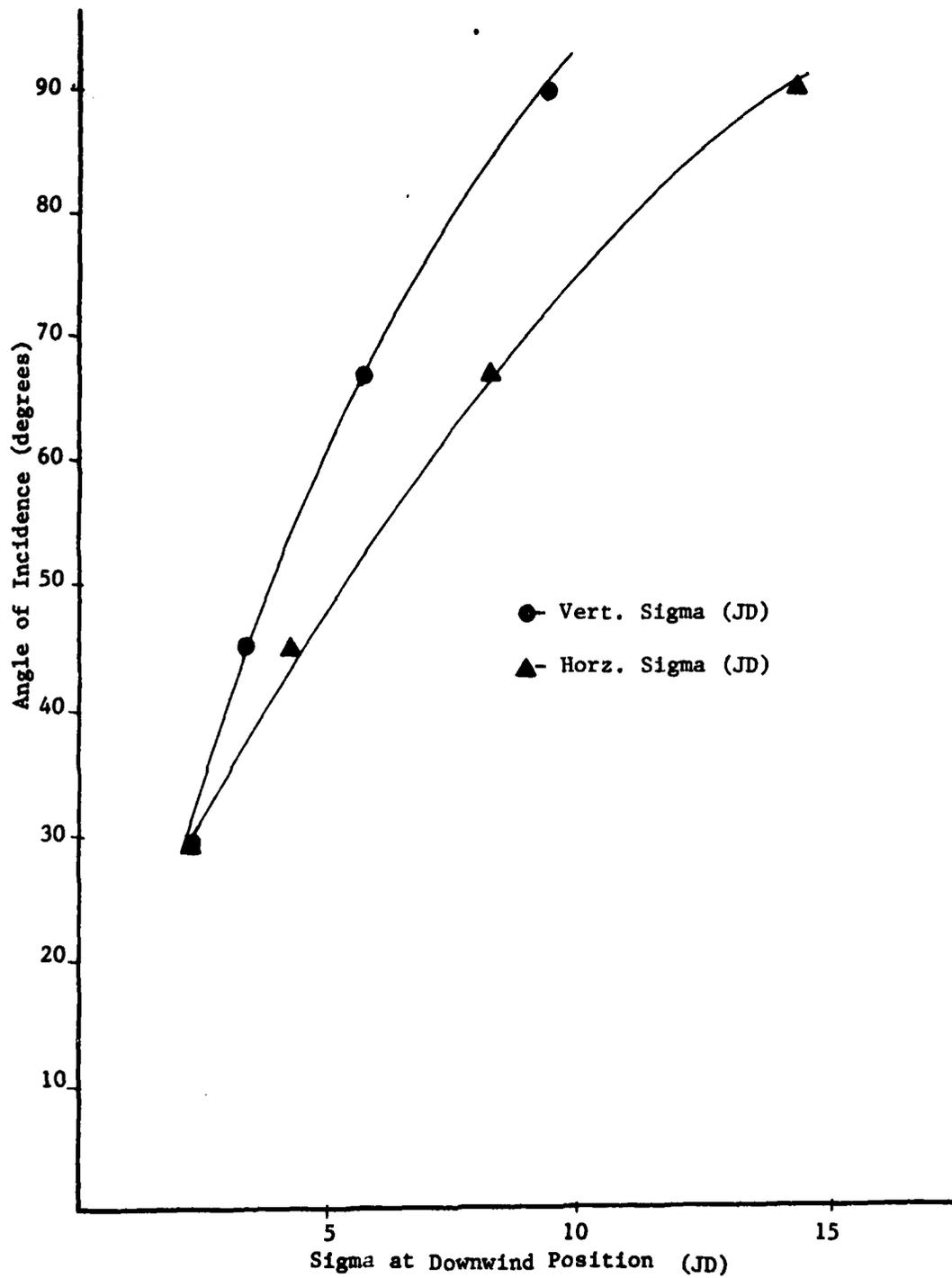
Figure 40
1-Sigma Width of Plume At Gaussian Position
vs. Angle of Incidence to the Wind

V. REFERENCES

1. Rote, D. M. and Wangen, L. E., "A Generalized Air Quality Assessment Model for Air Force Operations," Air Force Weapons Laboratory Report AFWL-TR-74-304, February 1975.

2. Rote, D. M., and Wangen, L. E., A Generalized Air Quality Assessment Model for Air Force Operations--An Operators Guide," Air Force Weapons Laboratory Report AFWL-TR-74-54, June 1974.

3. Bingaman, D. J., "Air Quality Assessment Model for Air Force Operations, Short Term Emission/Dispersion Computer Code Documentation," Civil and Environmental Engineering Development Office (Air Force Systems Command) Report CEEDO-TR-76-34, April 1977.

4. Weal, K. I., and Netzer, D. W., "Modification of An Ambient Air Quality Model for Assessment of U. S. Naval Aviation Emittants," Naval Postgraduate School Report NPS-57Nt-75071A, August 1975.

5. Thompson, G. and Netzer, D. W., "An Ambient Air Quality Model for Assessment of U. S. Naval Aviation Emittants, "Naval Postgraduate School Report NPS-67Nt-76091, September 1976.

6. Music, P. D., Hunt, J. S., and Naugle, D. F., "Photographic Measurements of USAF Aircraft Plume Rise," Civil and Environmental Engineering Development Office (Air Force Systems Command) Report CEEDO-TR-77-57, November 1977.

7. Sundaram, T. R. and Ludwig, G. R., "On the Laboratory Simulation of Small Scale Atmospheric Turbulence," Cornell Aeronautical Laboratory, Inc. Report VC-2740-5-1, December 1969.

8. Sundaram, T. R., Ludwig, G. R., and Skinner, C. T., "Modeling of the Turbulence Structure of the Atmospheric Surface Layer," AIAA Journal Vol. 10, No. 6, p. 743-750, June 1972.

9. Cermak, J. E., "Laboratory Simulation of the Atmospheric Boundary Layer," AIAA Journal Vol. 9, No. 9, p. 1746-1753, September 1971.

10. Cermak, J. E., "Applications of Fluid Mechanics to Wind Engineering, A Freeman Scholar Lecture", paper presented at the Winter Annual Meeting of the American Society of Mechanical Engineers, New York, N.Y., 17-21 November 1974.

11. Chaudhry, F. H. and Cermak, J. E., "Wind Tunnel Modeling of Flow and Diffusion Over an Urban Complex," Fluid Mechanics Program, Engineering Research Center, College of Engineering, Colorado State University Project THEMIS Report TR-17, May 1971.

12. Kawatani, T., and Sadeh, W. Z, "An Investigation of Flow Over High
    Roughness," Fluid Mechanics Program, Engineering Research Center,
    College of Engineering, Colorado State University, Project THEMIS
    Report TR-11, August 1971.

13. Huang, Chin-hua, and Nickerson, E. C., "Numerical Similation of Wind,
    Temperature, Shear Stress, and Turbulent Energy Over Non-Homogeneous
    Terrain," Fluid Mechanics Program, Engineering Research Center,
    College of Engineering, Colorado State University, Project THEMIS
    Report TR-12, p. 21-28, March 1972.

14. Monin, A. S. and Obukhov, A. M., "Basic Regularity in Turbulent Mix-
    ing in the Surface Layer of the Atmoshpere," USSR Acad. Sci. Works
    of Geophysics Met., No. 24 p. 163, 1954.

15. Schlichting, H., Boundary Layer Theory, McGraw Hill, 1955.

16. Turner, D. B., "Workbook of Atmoshperic Dispersion Estimates,"
    U.S. Dept. of Health, Education, and Welfare, U.S. Public Health
    Service Publication No. 999-AP-26, January 1974.

DISTRIBUTION LIST

No. of Copies

1. Chief of Naval Operations   2
   Navy Department
   Washington, DC 20760
   (Attn: Codes: OP451, OP453)

2. Chief of Naval Material   2
   Navy Department
   Washington, DC 20360
   (Attn: Codes: 08T291, 055P1)

3. Commander   8
   Naval Air Systems Command
   Washington, DC 20361
   (Codes: AIR-01B, 330D, 340E, 4147A,
   50184, 5341B, 536B1, 53645)

4. Commander   1
   Naval Air Force
   U.S. Pacific Fleet
   Naval Air Station
   North Island
   San Diego, CA 92135
   (Code: 722)

5. Commanding Officer   1
   Naval Air Rework Facility
   Naval Air Station North Island
   San Diego, CA 92135
   (Code: 64270)

6. Commander   2
   Naval Facilities Engineering Command
   200 Stoval Street
   Alexandria, VA 22332
   (Codes: 104, 032B)

7. Commanding Officer   1
   Naval Facilities Engineering Command
   Western Division
   San Bruno, CA 94066
   (Code: 09BE)

8. Naval Construction Battalion Center   3
   Port Hueneme, CA 93043
   (Codes 25, 251, 252)

9. U.S. Naval Academy   1
   Annapolis, MD 21402
   (Attn: Prof. J. Williams)

10. U.S. Marine Corps   1
    Washington, DC 20380
    (Attn: Code: AAJ)

11. U.S. Air Force   1
    Washington, DC 20330
    (Attn: Code PREV)

12. Arnold Engineering Development Ctr.   1
    Arnold AFS, TN 37342
    (Code: DYR)

13. Air Force Aero Propulsion Laboratory   1
    Wright-Patterson Air Force Base, OH 45433
    (Code: SFF)

14. Detachment 1   2
    Civil & Environmental Eng. Dev. Agency
    HQ ADTC/ECA
    Tyndall AFB, TN 32403
    (Code: EV, EVA)

15. Air Force School of Aerospace Medicine   1
    Brooks, AFB, TX 78235
    (Code: VNL)

16. Army Aviation Systems Command   1
    P.O. Box 209
    St. Louis, MO 63166
    (Code: EQP)

17. Eustis Directorate   1
    USA AMR & DL
    Ft. Eustis, VA 23604
    (Code: SAVDL-EU-TAP)

18. National Aeronautics and Space Admin.   1
    Lewis Research Center
    2100 Brookpark Road
    Cleveland, OH 44135
    (Attn: Mail Stop 60-6 (R. Rudey))

19. National Aeronautics and Space Administration   1
    Langley Research Center
    Hampton, VA 23365
    (Attn: Mail Stop 217K, Dr. Levine)

20. Environmental Protection Agency   1
    401 M. Street, S.W.
    Washington, DC 20024
    (Attn: G. Kittredge)

21. Environmental Protection Agency   1
    Procedures Development Branch
    2565 Plymouth Road
    Ann Arbor, MI 48105
    (Attn: D. Munt)

22. Environmental Protection Agency   1
    National Environmental Research Center
    Meteorology Laboratory
    Research Triangle Park, NC 27711
    (Attn: P. Humphry)

23. Environmental Protection Agency   2
    National Environmental Research Center
    P. O. Box 15027
    Las Vegas, NV 89114
    (Attn: Mr. Snelling)

24. Federal Aviation Administration   2
    800 Independence Avenue, SW
    Washington, DC 20590
    (Code AEQ-10; A. Broderick)

25. Federal Aviation Administration   1
    2100 2nd Street
    Washington, DC 20591
    (Code: ARD550, W. Westfield)

26. Federal Aviation Administration   1
    National Aviation Facility Experimental Ctr.
    Atlantic City, NJ 08405
    (Code: ANA-420)

27. Defense Documentation Center   2
    Cameron Station
    Alexandria, VA 22314

28. Naval Air Propulsion Center   3
    Trenton, NJ 08608
    (Attn: A. Klarman, Code PE71:AK)

29. Library   2
    Code 0142
    Naval Postgraduate School
    Monterey, CA 93940

30. Dept. of Aeronautics
    Code 67
    Monterey, CA 93940
       M. F. Platzer, Chairman   1
       D. W. Netzer   10